symmetry

IMPACT FACTOR 2.2

CITESCORE 5.4

Review

Symmetry-Related Topological Phases and Applications: From Classical to Quantum Regimes

Rui Zhang and Tian Chen

Special Issue

Symmetry/Asymmetry in Topological Phases

Edited by

Dr. Tian Chen, Prof. Dr. Daohong Song and Prof. Dr. Fuchuan Lei

MDPI

https://doi.org/10.3390/sym16121673

symmetry

MDPI

Review

Symmetry-Related Topological Phases and Applications: From Classical to Quantum Regimes

Rui Zhang [1,*] and Tian Chen [2,*]

[1] National Engineering Laboratory for Public Safety Risk Perception and Control by Big Data, China Academy of Electronics and Information Technology, Beijing 100041, China
[2] Beijing Key Laboratory of Nanophotonics and Ultrafine Optoelectronic Systems, School of Physics, Beijing Institute of Technology, Beijing 100081, China
* Correspondence: zhangrui34@cetc.com.cn (R.Z.); chentian@bit.edu.cn (T.C.)

Abstract: Topological phase has received considerable attention in recent decades. One of the crucial factors to determine the phase is symmetry. Such a concept involves mathematical, geometrical, and physical meanings, which displays many fascinating phases in Hermitian and non-Hermitian systems. In this paper, we first briefly review the symmetry-related topological phases in Hermitian and non-Hermitian systems. The study in this section focuses on the topological phase itself, not the realizations therein. Then, we present a thorough review of the observations about these symmetry-related topological phenomena in classical platforms. Accompanied by the rise of quantum technology, the combination of symmetry-related topological phase and quantum technology leads to an additional new avenue, in which quantum information tasks can be accomplished better. Finally, we provide comments about future research into symmetry-related topological phases.

Keywords: symmetry; topological phase; classical and quantum platforms; applications

Citation: Zhang, R.; Chen, T. Symmetry-Related Topological Phases and Applications: From Classical to Quantum Regimes. *Symmetry* **2024**, *16*, 1673. https://doi.org/10.3390/sym16121673

Academic Editor: Manuel Gadella

Received: 11 November 2024
Revised: 9 December 2024
Accepted: 13 December 2024
Published: 17 December 2024

1. Introduction

Symmetry refers to the property of a system that remains unchanged after performing certain operations, such as rotation, reflection, and translation, among others. In physics, symmetry is often closely related to conservation laws; for example, spatial translational symmetry corresponds to the law of momentum conservation, spatial rotational symmetry is closely related to the law of angular momentum conservation, and time-reversal symmetry has a one-to-one correspondence to the law of energy conservation [1–17]. When distinguished by type, symmetry includes spatial symmetry, time-reversal symmetry, and intrinsic symmetry. Spatial symmetry refers to the property of an object that remains unchanged under spatial transformations, including translational symmetry, rotational symmetry, and reflective symmetry. Time-reversal symmetry refers to the unchanged property during time evolution and can be further divided into static symmetry and dynamic symmetry. Intrinsic symmetry describes the property of an object that remains unchanged under certain internal transformations, involving the fundamental particles and their interactions.

Topological phase refers to a special state of matter, characterized by its properties that do not depend on the specific shape and size, but only on its intrinsic structure. The structure of matter is closely related to symmetries, such as translational symmetry that occurs in periodic lattice systems, as well as symmetry points, symmetry lines, and symmetry planes in the unit cells of lattice systems. In order to accurately describe the relationship between topology and symmetry, researchers approach it from the perspective of group theory and use various mathematical tools to analyze the topological properties under different symmetries. They have found that when only chiral symmetry, time-reversal symmetry, and particle-hole symmetry are present, lattice systems can be classified into ten different categories [17]. But when mirror symmetry is introduced, there are far

more than ten kinds of topologies. When non-Hermitian couplings are introduced into lattices, the topological classification characterized by symmetry becomes more diverse [18]. These detailed reviews will be introduced in Section 2.

Not only are mathematical descriptions of symmetry and topological phases rapidly developing, but researchers are also seeking ways to demonstrate topological phenomena in practical physical systems. In our review, we will first focus on how to observe physical phenomena in classical systems. These classic systems mainly involve optical, electrical, mechanical, and acoustic systems. In these systems, researchers have cleverly designed and demonstrated topological phenomena corresponding to the description of symmetry. Next, we will focus on topological phenomena in quantum systems. Due to special quantum effects, such as quantum decoherence, the topological properties of quantum systems are not exactly the same as those of classical systems. In this review, we take quantum open systems as an example and provide a brief introduction to their topological phenomena by combining quantum jump transitions. The relevant reviews are placed in Section 3. It is worth noting that due to the existence of a large number of works on topology, we cannot cite all of them in this review. During our writing, we only selected some of the representative early studies. Additional studies can be found in the references of the cited literature.

Furthermore, we also focus on the practical applications of topological phases. By combining the unique topological structure of exceptional points, chiral energy and information transmission can be achieved, and energy and information output can be generated at specific ports. In particular, the robustness brought by topological properties enables energy and information transmission in a stable way, even in the presence of external disturbances. This topological property can also be used for applications such as quantum information. With the help of constructed topological structures, such as exceptional points, chiral quantum state transmission can be achieved. A corresponding review will be conducted in Section 4.

Based on the rapidly developing topological properties and their applications, we provide a summary and outlook at the end, in Section 5. In the summary, we make a connection between topology and symmetry, as well as the description of novel topological properties at present. In the outlook, we focus on various platforms for observing topological phases and their possible applications.

2. Symmetry

In this section, we review how different symmetries can be achieved in Hermitian and non-Hermitian fermionic systems. We are now considering a general non-interacting system composed of fermions, described by a second-order quantized Hamiltonian $\hat{H}$. For a non-superconducting system, $\hat{H}$ can be written as

$$\hat{H} = \hat{\Psi}_I^\dagger H^{IJ} \hat{\Psi}_J \equiv \hat{\Psi}^\dagger \hat{H} \hat{\Psi} \tag{1}$$

Here, $\hat{\Psi}_I^\dagger$ and $\hat{\Psi}_J$ are creation and annihilation operators of fermions, I and J are composite labels of lattice sites $i, j, \ldots$, and quantum numbers. For example, $I = (i, \sigma)$ with $\sigma = \pm 1/2$, where $\hat{\Psi}_I^\dagger$ and $\hat{\Psi}_J$ satisfy the relation $\{\hat{\Psi}_J, \hat{\Psi}_I^\dagger\} = \delta_{IJ}$, H^{IJ} is the first-order quantized Hamiltonian matrix. Similarly, for superconducting systems described by the Bogoliubov–de Gennes (BdG)–Hamiltonian matrix, the Nambu spin is used instead of the fermion operator, and the first-order quantized Hamiltonian in the lattice system remains the matrix H. Next, we discuss explicitly the formed topological phases under three fundamental symmetries, time-reversal, particle-hole, and chiral symmetries. More properties of other symmetries and related topological phases can be found in Ref. [13].

2.1. Symmetry of Hermitian Systems

2.1.1. Time-Reversal Symmetry (TRS)

Time-reversal symmetry (TRS) is an important property in physics. It describes the symmetry exhibited by a physical system under time reversal operations; that is, if the

motion process of a physical system is recorded and reversed, the system still obeys the same physical laws. Considering TRS, the time reversal operator $\hat{T}$ is a non-unitary operator, which acts on fermionic systems as follows:

$$\hat{T}\hat{\Psi}_I\hat{T}^{-1} = (U_T)_I{}^J\hat{\Psi}_J, \hat{T}i\hat{T}^{-1} = -i. \tag{2}$$

If a system preserves the canonical anticommutator $\left\{\hat{\Psi}_I, \hat{\Psi}_J^\dagger\right\} = \hat{T}\left\{\hat{\Psi}_I, \hat{\Psi}_J^\dagger\right\}\hat{T}^{-1}$ and $\hat{H}$ satisfies $\hat{T}\hat{H}\hat{T}^{-1} = \hat{H}$ under operation $\hat{T}$, then this system is TR invariant.

According to TRS, we can obtain the Hermitian matrix operator $\hat{o}$ to satisfy the fermionic system $\hat{T}\hat{o}(t)\hat{T}^{-1} = \hat{T}e^{+i\hat{H}t}\hat{o}e^{-i\hat{H}t}\hat{T}^{-1} = \hat{o}(-t)$, and for generic non-interacting systems, $\hat{T} : U_T^\dagger H^* U_T = +H$ and $(U_T^* U_T)^\dagger H(U_T^* U_T) = H$. Considering U_T as a unitary matrix, then $U_T^* = e^{i\alpha}U_T^\dagger \Rightarrow (U_T)^T = e^{i\alpha}U_T$. We can obtain $e^{2i\alpha} = 1$, and $U_T^* U_T = \pm\mathbb{I}$. Therefore, by applying $\hat{T}^2$ to the fermion operator $\hat{\Psi}_I$, we can obtain $\hat{T}^2\hat{\Psi}_I\hat{T}^{-2} = \left(U_T^* U_T\hat{\Psi}\right)_I = \pm\hat{\Psi}_I$. Similarly, for a general system composed of N fermions, one can also obtain the following:

$$\hat{T}^2 = (\pm 1)^{\hat{N}}, \text{ when } U_T^* U_T = \pm\mathbb{I}, \tag{3}$$

where the total fermion number operator $\hat{N} := \Sigma_I\hat{\Psi}_I^\dagger\hat{\Psi}_I$. When $U_T^* U_T = -\mathbb{I}$, $\hat{T}^2$ is the fermion number parity operator $\hat{\mathcal{G}}_f := (-1)^{\hat{N}}$. For a system with an odd number of fermions $\hat{T}^2 = -1$, the eigenvalues of fermion systems that satisfy TR invariance exhibit Kramers' degeneracy theorem.

2.1.2. Particle-Hole Symmetry (PHS)

Another important symmetry is particle-hole symmetry (PHS). It points out that in a physical system, the excitation of particles and holes has a certain symmetry. Specifically, if the Hamiltonian mechanics of a system exhibit invariance under some kind of transformation between particles and holes, then the system is said to have PHS. When referring to the fermion system, the unitary transformation of the particle hole (PH) operator $\hat{\mathcal{C}}$ on the fermion system is provided as follows:

$$\hat{\mathcal{C}}\hat{\Psi}_I\hat{\mathcal{C}}^{-1} = (U_C^*)_I{}^J\hat{\Psi}_J^\dagger. \tag{4}$$

The operator $\hat{\mathcal{C}}$ is also called the charge conjugation operator, in particle-number conserving systems $\hat{\mathcal{C}}\hat{Q}\hat{\mathcal{C}}^{-1} = -\hat{Q}$, where $\hat{Q} := \hat{N} - N/2$ and $N/2$ is half the number of orbits, i.e., half the dimension of a single particle Hilbert space.

Imagine a fermion system is PHS, the matrix U_C is unitary when the canonical anticommutation relation is invariant. And for non-interacting systems, $\hat{H} = \hat{\mathcal{C}}\hat{H}\hat{\mathcal{C}}^{-1} = -\hat{\Psi}^\dagger\left(U_C^\dagger H^T U_C\right)\hat{\Psi} + \mathrm{Tr}H$, there can be $\hat{\mathcal{C}} : U_C^\dagger H^T U_C = -H$. $\mathrm{Tr}H = H^{II} = 0$. Consider a Hermitian system composed of a single fermion, which satisfies the PHS condition and can be written as $-U_C^\dagger H^* U_C = H$. In a single particle Hilbert space, condition $\hat{\mathcal{C}}$ is not unitary symmetry, but rather a reality condition on the Hamiltonian H modulo unitary rotations. Similar to the derivation of TRS in the previous section, we can also obtain

$$\hat{\mathcal{C}}^2 = (\pm 1)^{\hat{N}}, \text{ when } U_C^* U_C = \pm\mathbb{I} \tag{5}$$

For the PHS system, the eigenstate of $\hat{H}$ under action $\hat{\mathcal{C}}$ remains the same, since $\hat{\mathcal{C}}\hat{H}\hat{\mathcal{C}}^{-1}\left|\alpha\right\rangle = E_\alpha\hat{\mathcal{C}}\left|\alpha\right\rangle$. Considering a wave function with a single particle energy ε^A, $H^{IJ}u_J^A = \varepsilon^A u_I^A$, its particle-hole reversed partner $U_C^\dagger\left(u^A\right)^*$ is an eigenwave function with an energy $-\varepsilon^A$, since $U_C^\dagger H^* U_C U_C^\dagger\left(u^A\right)^* = \varepsilon^A U_C^\dagger\left(u^A\right)^*$.

2.1.3. Chiral Symmetry (CS)

Chiral symmetry (CS) refers to the existence of two independent spin states for particles with a spin of $1/2$, known as up and down states. If the interaction in which particles

participate is transformed by a certain symmetry group, and the transformation rules of up particles and down particles are different, then the symmetry reflected by the symmetry group is called CS. Moreover, the combination of $\hat{T}$ and $\hat{\mathcal{C}}$ leads to chiral symmetry (CS) $\hat{S} = \hat{T} \cdot \hat{\mathcal{C}} \cdot \hat{S}$, which acts on the fermion system as follows:

$$\hat{S}\hat{\Psi}_I \hat{S}^{-1} = (U_C U_T)_I{}^J \hat{\Psi}_J^\dagger \tag{6}$$

Under the chiral symmetry, the Hamiltonian H is invariant under $\hat{S}: U_S^\dagger H U_S = -H$ where $U_S = U_C^* U_T^*$ and $\mathrm{Tr}H = 0$. It can be obtained $U_S^2 = e^{i\alpha}\mathbb{I}$ with $\hat{T}^2 = \hat{\mathcal{C}}^2 = (\pm)^{\hat{N}}$. By redefining $U_S \to e^{i\alpha/2} U_S$, the chiral symmetry condition of a single particle Hamiltonian can be simplified to $\hat{S}: \{H, U_S\} = 0$, $U_S^2 = U_S^\dagger U_S = \mathbb{I}$ and the eigenvalues of the chiral operator are ± 1.

In this case, the energy spectrum of a single particle Hamiltonian is a symmetric spectrum: assuming that the eigenstate of H corresponding to the eigenvalue ε is $|u\rangle$, then $U_S|u\rangle$ is the eigenstate of H with the eigenvalue $-\varepsilon$. In the basis in which U_S is diagonal, H is a block off-diagonal:

$$H = \begin{pmatrix} 0 & D \\ D^\dagger & 0 \end{pmatrix},$$

where D is a $N_A \times N_B$ rectangular matrix and $N_A + N_B = N$. Consider a tight-binding Hamiltonian of spinless fermions on a bipartite lattice: $\hat{H} = \sum_{m,n} t_{mn} \hat{c}_m^\dagger \hat{c}_n$, $t_{mn} = t_{nm}^* \in \mathbb{C}$. Combining the particle-hole (PH) transformation $\hat{\mathcal{C}} \hat{c}_m \hat{\mathcal{C}}^{-1} = (-)^m \hat{c}_m$ and TRS transformation $\hat{T} \hat{c}_m \hat{T}^{-1} = \hat{c}_m$ ($\hat{T} i \hat{T} = -i$) of spinless fermions, chiral transformation $\hat{S} \hat{c}_m \hat{S}^{-1} = (-)^m \hat{c}_m^\dagger$ and $\hat{S} i \hat{S}^{-1} = -i$ can be obtained. It can be concluded that when t_{mn} is a bipartite hopping, i.e., when t_{mn} only connects the sites of different sublattices, $\hat{H}$ is invariant under $\hat{S}$. In addition to the bipartite hopping model, chiral symmetry also exists in QCD systems [1], BdG systems with TRS and S_z conservation [2], bosonic systems [3–5] and entanglement Hamiltonians [6–9].

2.1.4. BdG System

Next, we take the BdG system as an example and show the different types of topological phases under the three mentioned symmetries. Here, we provide a straightforward illustration of the characteristics of the Hamiltonian matrices and the corresponding properties of the states, when the system satisfies different symmetries. Then, we provide ten-fold different topological phases under these symmetries.

Class D

The Nambu spin quantity is expressed as follows:

$$\hat{Y} = \begin{pmatrix} \hat{\Psi}_I \\ \vdots \\ \hat{\Psi}_N \\ \hat{\Psi}_I^\dagger \\ \vdots \\ \hat{\Psi}_N^\dagger \end{pmatrix},$$

where $\hat{Y}^\dagger = \left(\hat{\Psi}_I^\dagger, \cdots, \hat{\Psi}_N^\dagger, \hat{\Psi}_I, \cdots, \hat{\Psi}_N\right)$ satisfies the canonical anticommutation relation as

$$\left\{\hat{Y}_A, \hat{Y}_B^\dagger\right\} = \delta_{AB} (A, B = 1, \cdots, 2N) \tag{7}$$

The operators $\hat{Y}$ and $\hat{Y}^\dagger$ are not independent of each other, and they satisfy the relation as $\left(\tau_1\hat{Y}\right)^T = \hat{Y}^\dagger$, $\left(\hat{Y}^\dagger\tau_1\right)^T = \hat{Y}$, where the Pauli matrix τ_1 acts on the Nambu space. The BdG–Hamiltonian matrix is represented by the Nambu spin quantity as follows:

$$\hat{H} = \frac{1}{2}\hat{Y}_A^\dagger H^{AB},\ \hat{Y}_A = \frac{1}{2}\hat{Y}^\dagger H\hat{Y}. \tag{8}$$

Since $\hat{Y}$ and $\hat{Y}^\dagger$ are not independence from each other, we have $\hat{H} = (1/2)\left(\tau_1\hat{Y}\right)^T H\left(\hat{Y}^\dagger\tau_1\right)^T = -(1/2)\hat{Y}^\dagger(\tau_1 H\tau_1)^T\hat{Y} + (1/2)\mathrm{Tr}(\tau_1 H\tau_1)$, and one can obtain the following:

$$\tau_1 H^T\tau_1 = -H. \tag{9}$$

That is to say, any single particle BdG–Hamiltonian matrix satisfies the PHS form. However, Equation (9) is generated by the intrinsic characteristics of the Fermi statistics of the BdG–Hamiltonian matrix and is not obtained by applying symmetry. Therefore, for the BdG system, Equation (9) should be referred to as particle-hole constraint or Fermi constraint [10]. The Hamiltonian ensemble that satisfies constraint Equation (9) is called class D. By applying different symmetries to the BdG–Hamiltonian matrix, five additional symmetry families, DIII, A, AIII, C, and CI, can also be obtained. According to Equation (9), the BdG–Hamiltonian matrix can be written as

$$H = \begin{pmatrix} \Xi & \Delta \\ -\Delta^* & -\Xi^T \end{pmatrix},$$

$\Xi = \Xi^\dagger$, $\Delta = -\Delta^T$, where Ξ represents the normal part and Δ is the anomalous part.

The BdG–Hamiltonian matrix can be considered as the single particle Hamiltonian of the Majorana fermions. Through the following:

$$\begin{pmatrix} \hat{\lambda}_I \\ \hat{\lambda}_{I+N} \end{pmatrix} = \begin{pmatrix} \hat{\Psi}_I + \hat{\Psi}_I^\dagger \\ i(\hat{\Psi}_I - \hat{\Psi}_I^\dagger) \end{pmatrix},$$

we can obtain the Majorana representation of the BdG–Hamiltonian matrix, where the Majorana fermions $\hat{\lambda}$ satisfy

$$\left\{\hat{\lambda}_A,\ \hat{\lambda}_B\right\} = 2\delta_{AB},\quad \hat{\lambda}_A^\dagger = \hat{\lambda}_A(A, B = 1, \cdots, 2N). \tag{10}$$

In the Majorana basis, the BdG–Hamiltonian matrix can be written as follows:

$$\hat{H} = i\hat{\lambda}_A X^{AB}\hat{\lambda}_B,\ \ X^* = X,\ \ X^T = -X \tag{11}$$

Here, the $4N \times 4N$ matrix is as follows:

$$iX = \frac{1}{2}\begin{pmatrix} R_- + S_- & -i(R_+ - S_+) \\ i(R_+ + S_+) & R_- - S_- \end{pmatrix},$$

where $R_\pm = \Xi \pm \Xi^T = \pm R_\pm^T$, $S_\pm = \Delta \pm \Delta^* = -S_\pm^T$. Matrix X can be transformed into block diagonal form through orthogonal transformation, i.e., $X = o\sum o^T$, $\sum = \begin{pmatrix} 0 & \varepsilon_1 & & & \\ -\varepsilon_1 & 0 & & & \\ & & \ddots & & \\ & & & 0 & \varepsilon_N \\ & & & -\varepsilon_N & 0 \end{pmatrix}$, where o is orthogonal and $\varepsilon_I \geq 0$. Under the rotation basis $\hat{\xi} := o^T\hat{\lambda}$, Hamiltonian $\hat{H} = i\hat{\xi}^T\sum\hat{\xi} = 2\sum_{I=1}^N \varepsilon_I\hat{\xi}_{2I-1}\hat{\xi}_{2I}$.

Although it is usually possible to rewrite the BdG–Hamiltonian matrix using the Majorana operator, Majorana eigenstates are rarely BdG–Hamiltonian eigenstates, i.e., unpaired or isolated Majorana zero-energy eigenstates only appear in very few special cases in BdG

systems. Furthermore, we found that, in general, one cannot directly represent complex Fermi operators using a series of given Majorana operators; thus it is impossible to directly rewrite the Majorana–Hamiltonian correlation in the form of a BdG–Hamiltonian matrix.

Class DIII

Let us consider the case of applying TRS operation $\hat{T}^2 = \hat{\mathcal{G}}_f$ on the BdG–Hamiltonian matrix, where the TR operator acts on the fermion operator as follows:

$$\hat{T}\hat{\Psi}_{I\sigma}\hat{T}^{-1} = (i\sigma_2)_{\sigma\sigma'}\hat{\Psi}_{I\sigma'}, \tag{12}$$

Here, the subscript is $\sigma = \uparrow / \downarrow$, spin, σ_2 is the Pauli matrix acting on the spin space. It can be concluded that the BdG–Hamiltonian matrix satisfies the constraints as follows:

$$\tau_1 H^T \tau_1 = -H,\ \sigma_2 H^* \sigma_2 = H. \tag{13}$$

It is easy to achieve H satisfies chiral symmetry $\tau_1\sigma_2 H \tau_1\sigma_2 = -H$. An ensemble of BdG–Hamiltonian matrices satisfying Equation (13) is called Class DIII. Similarly, for the $\hat{T}^2 = +1$ situation, Class BDI can be obtained.

Classes A and AIII

Next, we consider the BdG–Hamiltonian matrix with $U(1)$ spin-rotation symmetry around the S_Z axis in spin space as follows:

$$\hat{H} = \hat{\Psi}_A^\dagger\, H^{AB}\hat{\Psi}_B, \tag{14}$$

where H is a $2N \times 2N$ unconstrained matrix, and

$$\hat{\Psi}^\dagger = \begin{pmatrix} \hat{\Psi}^\dagger_{I\uparrow} & \hat{\Psi}_{I\downarrow} \end{pmatrix},\ \hat{\Psi} = \begin{pmatrix} \hat{\Psi}_{I\uparrow} \\ \hat{\Psi}^\dagger_{I\downarrow} \end{pmatrix} \tag{15}$$

Note that, unlike Nambu spin quantities, there is no constraint relationship between $\hat{\Psi}$ and $\hat{\Psi}^\dagger$, H is unconstrained and known as symmetry class A.

Let the operator $\hat{\Psi}^\dagger_\downarrow \to \hat{\Psi}_\downarrow$, the BdG system Equation (14) can be transformed into a general Fermi system with particle number conservation, and the $U(1)$ spin-rotation symmetry can be transformed into pseudocharge $U(1)$ symmetry. Apply TRS to the BdG–Hamiltonian matrix in Equation (14), we obtain the following:

$$\hat{T}\hat{\Psi}\hat{T}^{-1} = \begin{pmatrix} \hat{\Psi}_\downarrow \\ -\hat{\Psi}^\dagger_\uparrow \end{pmatrix} = i\rho_2\left(\hat{\Psi}^\dagger\right)^T =: \hat{\Psi}^C, \tag{16}$$

where $\rho_{1,2,3}$ represent the Pauli matrices that act on particle-hole and spin components. If we consider $\hat{\Psi}^\dagger_\uparrow \to \hat{\Psi}_\uparrow$, i.e., the conservation of particle number, then $\hat{T}$ in Equation (16) can form $\hat{T}$ and $\hat{\mathcal{C}}$, one can obtain chiral symmetry. In fact, the relationship between chiral symmetry $\hat{T}\hat{\mathcal{C}}$ and the $U(1)$ charge $\hat{Q}$ of the particle-number conservation system $\left(\hat{T}\hat{\mathcal{C}}\right)\hat{Q}\left(\hat{T}\hat{\mathcal{C}}\right)^{-1} = \hat{Q}$ is isomorphic to the TRS and the $\hat{S}_Z$ in the S_Z conserved BdG system $\hat{T}\hat{S}_Z\hat{T}^{-1} = \hat{S}_Z$. That is to say, by reinterpreting Equation (14) as a particle-number conserving system, applying TRS can result in chiral symmetry. The Hamiltonian ensemble that satisfies this chiral symmetry is called class AIII. Therefore, the BdG system with S_Z conservation and TRS belongs to symmetry class AIII.

Classes C and CI

We now study the $SU(2)$ spin-rotation symmetry on the BdG–Hamiltonian matrix. Consider a spin-rotation $\hat{u}_n^{\phi}$ by an angle of ϕ around the rotation axis n acting on a doublet $\left(\hat{\Psi}_{\uparrow}, \hat{\Psi}_{\downarrow}\right)^T$ as follows:

$$\begin{pmatrix} \hat{\Psi}_{\uparrow} \\ \hat{\Psi}_{\downarrow} \end{pmatrix} \rightarrow \hat{u}_n^{\phi} \begin{pmatrix} \hat{\Psi}_{\uparrow} \\ \hat{\Psi}_{\downarrow} \end{pmatrix}, \ \hat{u}_n^{-\phi} = e^{-i(\phi/2)\sigma \cdot n} \begin{pmatrix} \hat{\Psi}_{\uparrow} \\ \hat{\Psi}_{\downarrow} \end{pmatrix}. \tag{17}$$

For an operation of spin rotation by ϕ around S_x or S_y axis, $\hat{\Psi}$ can be transformed into

$$\hat{u}_{S_x}^{\phi} \hat{\Psi} \hat{u}_{S_x}^{-\phi} = \cos(\phi/2)\hat{\Psi} - i\sin(\phi/2)\hat{\Psi}^C,$$

$$\hat{u}_{S_y}^{\phi} \hat{\Psi} \hat{u}_{S_y}^{-\phi} = \cos(\phi/2)\hat{\Psi} - i\sin(\phi/2)\hat{\Psi}^C \tag{18}$$

Specifically, when ϕ is π, there is $\hat{\Psi} \rightarrow -i\hat{\Psi}^C$ or $-\hat{\Psi}^C$, which is the discrete PH transformation. That is to say, if we consider Equation (14) in the system of particle-number conservation, $\hat{u}_{S_i}^{\pi} \hat{S}_Z \hat{u}_{S_i}^{-\pi} = -\hat{S}_Z$, $i = x, y$ can be regarded as charge complex conjugation $\hat{\mathcal{C}}\hat{Q}\hat{\mathcal{C}}^{-1} = -\hat{Q}$. Actually, $\hat{u}_{S_i}^{\pi}$ is a PH transformation with a square of -1, which is opposite to the PH constraint of class D. For a single particle Hamiltonian H, it can be obtained from rotation symmetry $\hat{u}_{S_i}^{\pi}$ that

$$\rho_2 H^T \rho_2 = -H \tag{19}$$

The Hamiltonian ensemble that satisfies condition Equation (19) is called class C. We note that for a quadratic Hamiltonian, the constraint of rotation symmetry $\hat{u}_{S_i}^{\pi}$ corresponds to a complete $SU(2)$ spin-rotation symmetry. This is because for any $SU(2)$ rotation, the Hamiltonian H is transformed into $\hat{\Psi}^{\dagger} H \hat{\Psi}$, and the complex conjugate is $\hat{\Psi}^{C\dagger} H \hat{\Psi}^C$ (i.e., $\hat{H} \rightarrow \alpha \hat{\Psi}^{\dagger} H \hat{\Psi} + (1-\alpha)\hat{\Psi}^{C\dagger} H \hat{\Psi}^C$). It can be inferred from $\hat{\Psi}^{\dagger} H \hat{\Psi} = \hat{\Psi}^{C\dagger} H \hat{\Psi}^C$ and the S_Z invariance that the BdG–Hamiltonian matrix exhibits $SU(2)$ spin-rotation symmetry.

Further, application of TRS operation Equation (16) yields $\hat{\Psi}^{\dagger} H \hat{\Psi} \rightarrow \hat{\Psi}^T \rho_2 H^* \rho_2 \left(\hat{\Psi}^{\dagger}\right)^T = -\hat{\Psi}^{\dagger} \rho_2 H^{\dagger} \rho_2 \hat{\Psi} = \hat{H}$, i.e., $\rho_2 H^{\dagger} \rho_2 = -H$. Combining PHS Equation (19), we can obtain the following:

$$\rho_2 H^T \rho_2 = -H, \ H^* = H. \tag{20}$$

The Hamiltonian ensemble that satisfies condition Equation (20) is called class CI.

2.1.5. Ten-Fold Symmetry

We now discuss the non-unitary symmetry classification of single particle Hamiltonian. Consider the following set of discrete symmetries:

$$\begin{aligned} T^{-1} H T = H, \quad & T = U_T \mathcal{K}, \quad U_T U_T^* = \pm \mathbb{I}, \\ C^{-1} H C = -H, \quad & C = U_C \mathcal{K}, \quad U_C U_C^* = \pm \mathbb{I}, \\ S^{-1} H S = -H, \quad & S = U_S, \quad U_S^2 = \mathbb{I}, \end{aligned} \tag{21}$$

$\mathcal{K}$ is a complex conjugate operator. Under non-unitary symmetry Equation (21), there are only 10 possible Hamiltonian H symmetry transformations.

Firstly, there are three possibilities for the transformation of H under TRS: (1) H is not TR invariant, i.e., $T = 0$ in Table 1; (2) H is TR invariant and $\hat{T}$ squares to 1, i.e., $T = 1$; (3) H is TR invariant and $\hat{T}$ squares to -1, i.e., $T = -1$. Similarly, there are three transformations of H under PHS, i.e., $C = 0$, +1, and -1. Therefore, there are nine possibilities for how H can transform under TRS and PHS.

Table 1. Periodic Table of Topological Insulators and Superconductors. $\delta := d - D$, where d is the spatial dimension and $D + 1$ is codimension of defect; The leftmost column represents the ten-fold symmetry classification of Fermi–Hamiltonian systems, with time inversion T, particle-hole C, chiral S, and different types of symmetries represented by +1 and -1. $\mathbb{Z}, \mathbb{Z}_2, 2\mathbb{Z}$ and 0 represent the presence or absence of nontrivial topological insulators, superconductors, or topological defects, as well as their existing states. $D = 0$ ($\delta = d$) is corresponding to the tenfold classification of gapped bulk topological insulators and superconductors [13]. Reproduced with permission [13] Copyright 2016, American Physical Society.

				δ							
Class	***T***	***C***	***S***	**0**	**1**	**2**	**3**	**4**	**5**	**6**	**7**
A	0	0	0	$\mathbb{Z}$	0	$\mathbb{Z}$	0	$\mathbb{Z}$	0	$\mathbb{Z}$	0
AIII	0	0	1	0	$\mathbb{Z}$	0	$\mathbb{Z}$	0	$\mathbb{Z}$	0	$\mathbb{Z}$
AI	1	0	0	$\mathbb{Z}$	0	0	0	$2\mathbb{Z}$	0	$\mathbb{Z}_2$	$\mathbb{Z}_2$
BDI	1	1	1	$\mathbb{Z}_2$	$\mathbb{Z}$	0	0	0	$2\mathbb{Z}$	0	$\mathbb{Z}_2$
D	0	1	0	$\mathbb{Z}_2$	$\mathbb{Z}_2$	$\mathbb{Z}$	0	0	0	$2\mathbb{Z}$	0
DIII	-1	1	1	0	$\mathbb{Z}_2$	$\mathbb{Z}_2$	$\mathbb{Z}$	0	0	0	$2\mathbb{Z}$
AII	-1	0	0	$2\mathbb{Z}$	0	$\mathbb{Z}_2$	$\mathbb{Z}_2$	$\mathbb{Z}$	0	0	0
CII	-1	-1	1	0	$2\mathbb{Z}$	0	$\mathbb{Z}_2$	$\mathbb{Z}_2$	$\mathbb{Z}$	0	0
C	0	-1	0	0	0	$2\mathbb{Z}$	0	$\mathbb{Z}_2$	$\mathbb{Z}_2$	$\mathbb{Z}$	0
CI	1	-1	1	0	0	0	$2\mathbb{Z}$	0	$\mathbb{Z}_2$	$\mathbb{Z}_2$	$\mathbb{Z}$

Further, we consider the properties of Hamiltonian under product action $S = T{\cdot}C$. In the presence of TRS or PHS, there are eight possibilities corresponding to $S = T{\cdot}C$ equals 0 or 1. In the absence of TRS and PHS, there is also an additional possibility corresponding to $S = 0$ or 1. Therefore, there are $(3 \times 3 - 1) + 2 = 10$ symmetries, as shown in Table 1. Table 1 shows the periods of topological insulators and superconductors; the first column of the table corresponds to these ten symmetries, which are also the framework used to classify topological insulators and superconductors. In Table 1, $\mathbb{Z}, \mathbb{Z}_2, 2\mathbb{Z}$ and 0 represent the presence or absence of nontrivial topological insulators, superconductors, or topological defects, as well as their existing states. The case of $D = 0$ ($\delta = d$) corresponds to the ten-fold classification of gapped bulk topological insulators and superconductors. The ten-fold symmetry extends the famous "threefold way" scheme of Wigner and Dyson, it was first proposed in Altland and Zirnbauer's article on disordered systems [11,12], and is therefore also known as the Altland–Zirnbauer (AZ) symmetry classes.

2.2. Symmetry of Non-Hermitian Systems

2.2.1. Non-Hermitian Topological Classification

In Hermitian systems, the gapped characteristics of topological insulators/superconductors are determined by the condition $\det H(k) \neq 0$, i.e., there is no zero energy in the bulk spectrum, where k is the momentum on the sphere or torus [14–17]. For non-Hermitian–Hamiltonian $H(k)$, Kawabata et al. defined their gapped phases under the same conditions [18]. These complex energy gaps are called point gaps (Figure 1a). The topological classification of point-gapped phases is given by the K-theoretical classification of the corresponding doubled Hermitian–Hamiltonian system as follows:

$$\widetilde{H}(k) := \begin{pmatrix} 0 & H(k) \\ H^{\dagger}(k) & 0 \end{pmatrix}, \tag{22}$$

Note that $\det H(k) \neq 0$ and $\det \widetilde{H}(k) \neq 0$ are equivalent. This classification scheme is applied to the 38-fold Bernard–LeClair classification [18,19]. In addition to point gaps, there is another type of non-Hermitian gapped structure [18] called the real/imaginary line-gapped phase (Figure 1a). In this case, the gapped phase is defined as a spectral structure with non-zero real/imaginary parts. Furthermore, the concept of line gap can be extended to several spectral islands on the complex energy plane.

In the situation of Hermitian classification, the classification of nontrivial phases corresponds to a topological insulator/superconductor, where the bulk nontrivial topology represents a topological gapless boundary mode. In fact, the real/imaginary line-gapped phase can be adiabatically associated with the Hermitian/anti-Hermitian gapped Hamiltonian systems without breaking symmetry or closing the line gap [18–21]. Therefore, the nontrivial topology of the line-gapped phase is essentially the same as that of the Hermitian gapped phase. The situation of point-gapped phase is completely different, as the doubled Hermitian–Hamiltonian $\widetilde{H}$ corresponding to the bulk-boundary in nontrivial topology does not correspond to the original Hamiltonian H, and there is no unified physical explanation for the point-gapped phase. However, in the absence of symmetry or only with transpose type TRS ($TT^* = \pm 1$), i.e., classes A, AI†, and AII† [18], the symmetry-protected skin effect provides a physical explanation for the topological classification of point gaps. The classification of skin effect in these three types is represented by the red font in Table 2. The above discussion does not mean that the symmetry-protected skin effect only occurs in A, AI†, and AII†, as topological invariants of these three classes may be non-zero in other classes.

Table 2. Topological classification of point gaps in AZ†, where red font represents skin-effect classification [18]. Reproduced and adapted from CC-BY open access publications American Physical Society.

				δ							
AZ†	***T***	***C***	***S***	**0**	**1**	**2**	**3**	**4**	**5**	**6**	**7**
A	0	0	0	0	$\mathbb{Z}$	0	$\mathbb{Z}$	0	$\mathbb{Z}$	0	$\mathbb{Z}$
AIII	0	0	1	$\mathbb{Z}$	0	$\mathbb{Z}$	0	$\mathbb{Z}$	0	$\mathbb{Z}$	0
AI†	1	0	0	0	0	0	$2\mathbb{Z}$	0	$\mathbb{Z}_2$	$\mathbb{Z}_2$	$\mathbb{Z}$
BDI†	1	1	1	$\mathbb{Z}$	0	0	0	$2\mathbb{Z}$	0	$\mathbb{Z}_2$	$\mathbb{Z}_2$
D†	0	1	0	$\mathbb{Z}_2$	$\mathbb{Z}$	0	0	0	$2\mathbb{Z}$	0	$\mathbb{Z}_2$
DIII†	-1	1	1	$\mathbb{Z}_2$	$\mathbb{Z}_2$	$\mathbb{Z}$	0	0	0	$2\mathbb{Z}$	0
AII†	-1	0	0	0	$\mathbb{Z}_2$	$\mathbb{Z}_2$	$\mathbb{Z}$	0	0	0	$2\mathbb{Z}$
CII†	-1	-1	1	$2\mathbb{Z}$	0	$\mathbb{Z}_2$	$\mathbb{Z}_2$	$\mathbb{Z}$	0	0	0
C†	0	-1	0	0	$2\mathbb{Z}$	0	$\mathbb{Z}_2$	$\mathbb{Z}_2$	$\mathbb{Z}$	0	0
CI†	1	-1	1	0	0	$2\mathbb{Z}$	0	$\mathbb{Z}_2$	$\mathbb{Z}_2$	$\mathbb{Z}$	0

2.2.2. Ten-Fold AZ† Symmetry Classes and Quantum Anomalies

In non-Hermitian cases, there are two types of TRS: complex-conjugate-type and transpose-type. Similarly, PHS with complex-conjugate-type and transpose-type can be defined. The ten-fold AZ symmetry class of Hermitian systems is defined by the combination of complex-conjugate-type TRS and transpose-type PHS; while the ten-fold AZ† classification of non-Hermitian systems is defined by the combination of transpose-type TRS and complex-conjugate-type PHS.

Lee et al. [22] pointed out that in AZ† symmetry class, the point-gap topological invariants of PBC curves can count the number of anomalous gapless modes with sufficiently large imaginary parts. Here, the D-dimensional anomalous gapless mode does not appear in the bulk of a lattice due to quantum anomalies but can appear in the D+1-dimensional Hermitian topological insulator/superconductor of the corresponding Hermitian AZ symmetry class. In linear dynamics described by non-Hermitian–Hamiltonian systems, eigenvalues with large imaginary parts are relevant to long-time dynamics. In this sense, the dynamics described by the point-gap nontrivial Hamiltonian are determined by the anomalous gapless mode of long-time dynamics. For example, the chiral modes appearing on the edges of quantum Hall insulators can describe the relevant modes in long-time dynamics of one-dimensional class A nontrivial systems (Figure 1b).

For the anomalous interpretation of non-Hermitian skin effect in classes A, AI† and AII†, a symmetry-protected skin effect gives a physical explanation for the nontrivial non-Hermitian topology under OBC, while anomalous gapless modes give the same effect under PBC. These facts all indicate an anomalous explanation for the symmetry-protected

skin effect, which is related to fermion production generated by quantum anomaly. For example, a traditional skin effect is related to the charge accumulation induced by chiral currents at the boundary. The anomalous explanation also provides a direct cause for the occurrence of high-dimensional skin effects in topological defects, with a typical example being the Rubakov–Callan effect (or monopole catalysis), which was first introduced as a mechanism for proton decay in the $SU(5)$ grand unified theory. The corresponding skin effect is realized in a class A three-dimensional Weyl–Hamiltonian system with valley-dependent dissipation in the presence of a magnetic monopole. In the Nielsen–Ninomiya theory [23], the chiral magnetic skin effect can be related to a typical fermion product mechanism, known as the chiral magnetic effect.

2.2.3. Non-Hermitian Topology and Degeneracy Points

In Hermitian topological classification, gapless structures in momentum space, such as Dirac and Weyl point/line nodes, are widely discussed [24–33]. In a D-dimensional space, a robust d-dimensional symmetry-protected gapless structure can be characterized by topological gap structures on the (D-d)-dimensional spheres surrounding the gapless structure. Based on the similar topological classification on the sphere, topological classification of point-gap and line-gap around the exceptional points is given in [34]. The parameterized non-Hermitian–Hamiltonian system at exceptional points is not diagonalized [35–37] (Figure 1c). Point/line gaps may open or close near exceptional points, as exceptional points are connected through a gapless structure called the bulk Fermi arc [34–41] (Figure 1c). Such topological classification utilizes various dimensions (such as exceptional points and rings) to describe symmetry-protected exceptional structures [38–53].

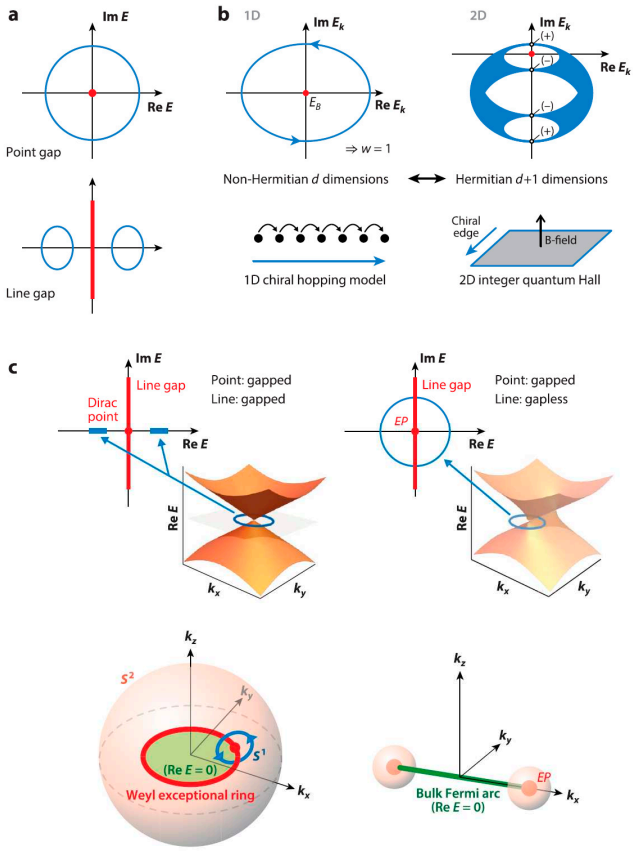

Figure 1. (**a**) Non-Hermitian gap spectrum (blue line). A point/line-gapped spectrum does not contain red points/lines. (**b**) The relation between Class-A point gap topology and chiral edge modes at the quantum Hall effect boundary. (**c**) Exceptional points (EPs) and their characteristics. Panels a–c adapted from reference [54]. Reproduced and adapted from CC-BY open access publications Annual Review.

3. Physical Implementations of Topological Phenomena

Researchers have used Hamiltonian mechanics to describe lattice systems and wave functions to describe the state of objects. However, since it does not involve the collective dynamics of multiple creation and annihilation operators, these Hamiltonians can actually be realized in classical systems. For example, in the propagation of optical waveguides, if the propagation direction is designed to be equivalent to time and the paraxial approximation is used, then the propagation of light along the waveguide has an equivalent form to the dynamics governed by the Schrödinger equation. In a circuit network, if the relationship between the voltage and current at each node is provided using an admittance matrix, then the voltage and current connected by such an admittance matrix can actually be regarded as the Schrödinger equation in the steady state. Other classical systems can also exhibit topological phenomena using their corresponding classical physical quantities through similar correspondences. In this part, we provide an overview of physical platforms ranging from classical systems to quantum systems. The explicit correspondences between the physical Hamiltonians and practical platforms are illustrated.

3.1. Classical System

In recent years, a large number of studies have demonstrated classical simulations of topological phases on a variety of experimental setups, including photons [55–57], electric circuits [58–60], and mechanical systems [61,62]. Due to the ubiquitous dissipation, these classical simulation experiments naturally occur in non-Hermitian situations. Classical systems can simulate quantum mechanics in many different ways: optical waveguides can directly simulate the time-dependent Schrödinger equation; the eigenmode problems of photonic crystals and acoustic systems can be equivalent to the Bloch problem of quantum systems with periodic potential. In circuits, the analogy is on the level of response functions, and quantum Hamiltonian can be directly simulated through an asymmetric dynamical matrix in robotic mechanical metamaterials.

3.1.1. Photonic System

We will focus on introducing photonic crystals, resonators, and coupled optical waveguides here.

Photonic crystals are metamaterials created by the spatially varying but periodic dielectric permittivity $\varepsilon_{ij}(x)$ and magnetic permeability $\mu_{ij}(x)$. Similar to electrons in crystalline solids, in photonic crystals, the electrodynamic eigenmodes of Maxwell's equations are subject to Bloch's theorem. Haldane and Raghu [55,56] proposed using photonic crystals to simulate quantum Hall states; Wang et al. conducted a series of refinements to this theory, realizing topological states in gyromagnetic photonic crystal and breaking the time-reversal symmetry [63,64]. In many photonic crystal experiments, non-Hermitian (NH) topological phenomena have been implemented, including the observation of Fermi arcs connecting exceptional points (EPs) [65]. The one-sided invisibility phenomenon of parity–time (PT) symmetric metamaterials [66] was observed, which was predicted to occur in PT-symmetric metamaterials operating at an EP [67–70]. Moreover, recent theoretical studies have pointed out that Maxwell waves, which exist on interfaces to separate lossless media with different signs in permittivity and permeability, have topological properties related to the NH helicity operator [71], further highlighting the NH characteristics of photonic crystals.

Photonic crystals form microresonators based on tiny defects in photonic crystals, which have a low Q factor. Whispering-gallery-mode resonators (WGMRs) are optical microresonators with a high Q factor, where electromagnetic waves are captured in the cavity due to total internal reflection. Peng et al. demonstrated unidirectional lasing [72,73] and single-mode lasing in PT-symmetric devices in NH experiments utilizing WGMRs [74,75], and improved sensitivity against perturbations in cavities operating at second-order EPs due to their nonanalytical dispersion behavior [76,77]. In addition, some researchers have studied the dynamical encircling of second-order EPs in microwave cavities [78], demonstrating experimental characteristics of mode switching.

Coupled optical waveguides provide another experimental platform for directly simulating the time evolution of tailor-made lattice models. In optical waveguides, Maxwell's equation describing the propagation of light along the z-axis, also known as the paraxial equation, is as follows:

$$i\partial_z \mathcal{E} = \left(-\frac{1}{2k_0}\left(\partial_x^2 + \partial_y^2\right) - \frac{k_0 \Delta n(x,y)}{n_0} \right) \mathcal{E}. \tag{23}$$

Equation (23) is formally equivalent to the two-dimensional Schrödinger equation, where z is playing the role of time t, the wave function $\mathcal{E}$ represents the envelope of the electric field polarized along the e, and $\mathrm{E}(x,y,z) = \mathcal{E}(x,y,z)e^{i(k_0 z - \omega t)}\mathrm{e}$ is assumed to vary slowly in the case of $|\nabla \mathcal{E}| \ll |k_0 E|$, $k_0 \approx k_z \gg k_{x,y}$. The effective potential $V(x,y) \propto \Delta n(x,y)$ can be tailor-made by using a femtosecond laser to carve waveguides, generating a strong spatially dependent local refractive index $\Delta n(x,y)$. Under the constraints of spatially sharp carving and weak evanescent coupling between waveguides, the system can be precisely constructed through a tight-binding Hamiltonian, whose hopping parameters depend on the device and the wavelength λ of light. It means that, when carefully designing the local refractive index $\Delta n(x,y)$, the Hamiltonians with different symmetries can be formed. Optical waveguides have been used to simulate Hermitian topological phases [79–82], including staggered gain and loss patterns in wires. The time evolution of effective NH models has also been successfully simulated, including experimental implementations of exceptional rings [83], defect states in NH–SSH chains [84], topological phase transitions [85], and PT-symmetric flat bands [86]. Research on the stability of corner states against gain and loss has also been proposed [87]. It is worth noting that only passive systems with staggered losses can generate such phases. Although energy is limited to lower complex half planes, a global shift can make the system effectively PT-symmetric, where waveguides with less loss are effectively converted to gain [88–92]. Regensburger et al. [93] achieved a true PT-symmetric system by using optical fibers, where PT-symmetric structures can be realized in the temporal domain using optical amplifiers and modulators. In addition, nonlinearity has been considered in the optical waveguides, and many new topological phases are uncovered [94–103].

3.1.2. Electric Circuit

The electric circuit provides another classic platform for implementing a non-Hermitian topology [58,59]. In electric circuits, people directly study the response function rather than the properties of Hamiltonian, where capacitors and inductors act as Hermitian elements, and resistors and amplifiers are non-Hermitian elements. For example, the current flowing through node i at frequency ω is as follows:

$$I_i(\omega) = \sum_j Y_{ij}(\omega) V_j(\omega), \tag{24}$$

where $I_i(\omega)$ and $V_i(\omega)$ are the input current and potential at node i, $Y_{ij}(\omega)$ is the admittance matrix, and the equivalent inverse impedance matrix is $\left[Z^{-1}(\omega)\right]_{ij}$. Specifically, $Y_{ij}(\omega)$ is the admittance between nodes i and j, and $Y_{ii}(\omega)$ is the admittance between node i and ground [59]. This relation can be derived using current conservation, which means that under Kirchhoff's circuit law, the total input current needs to be equal to the total output current. The current and voltage at the nodes of the circuit are as follows:

$$I_i(\omega) = \left[\mathrm{i}\omega C_{ij} + R_{ij}^{-1} + \left(\mathrm{i}\omega L_{ij}\right)^{-1}\right] \sum_{\langle j \rangle} \left[V_j(\omega) - V_i(\omega)\right] - \left[\mathrm{i}\omega C_{i0} + R_{i0}^{-1} + \left(\mathrm{i}\omega L_{i0}\right)^{-1}\right] V_i(\omega) \tag{25}$$

where I_i and V_i are the current and voltage of the node i with the angular frequency ω. The capacitance, resistance, and inductance between nodes i and j are expressed as C_{ij}, R_{ij} and L_{ij}. The corresponding electric component capacitance, resistance, and inductance between node i and ground are shown as C_{i0}, R_{i0} and L_{i0}. The label $\langle j \rangle$ means the summation over all electric nodes connected.

The periodicity of the circuit structure allows the use of Bloch's theorem to find the wave function, while the band structure of the circuit corresponds to the eigenvalues of admittance $Y_{ij}(\omega)$. In a circuit network, the voltage and current connected by such an admittance matrix can actually be regarded as the Schrödinger equation in the steady state, as follows:

$$Y(\omega)\begin{pmatrix}\cdots\\ V_i\\ \cdots\end{pmatrix} = 0 \tag{26}$$

In this way, the choices of different electric components, e.g., electric capacitance, inductance, and resistances, can determine the couplings in the admittance matrix, and that is the Hamiltonian matrix. Therefore, the admittance matrix $Y_{ij}(\omega)$ can be interpreted as a Hamiltonian matrix. By arranging capacitors, inductors, and other electronic building blocks, circuits that simulate the physical characteristics of topologically nontrivial models can be designed. Therefore, the Hamiltonian matrix with different symmetries can be uncovered. This idea was proposed by Ningyuan et al. [59] and has been used to construct topological circuits, whose band structure, i.e., admittance eigenvalues, also realizes the band topology structure of the Hofstadter model in Möbius strip devices [58,59]. Lee et al. [60] and Imhof et al. [104] reported the implementation of SSH chains and their two-dimensional extensions in circuits, as well as Weyl semimetal spectroscopy. Imhof et al. achieved angular states in two-dimensional circuit devices [104]. The implementation of these circuit-based Hermitian topological phases lays the foundation for their NH topological phase implementation. Helbig et al. [105] implemented the NH–SSH model using resistors and amplifiers and confirmed the theoretical predictions. Hofmann et al. also achieved the NH skin effect [106]. In addition, many ideas have been proposed based on circuit experimental platforms, including the use of PBC to implement NH honeycomb lattices [107], NH Chern insulators [108,109], high-order topological models [102] with NH skin states localized at low dimensional boundaries [110,111], and quantum walk simulations [112], the implementation of three-dimensional Seifert surfaces in four-dimensional circuits, and the implementation of pseudo magnetic fields to detect singular Landau energy levels in NH Dirac and Weyl systems [113,114]. Moreover, the high-order topological states, hybrid topological skin effect, and other topology are also revealed in the circuits [115–124].

3.1.3. Quantum Walk

Quantum walk provides another way to simulate and probe NH topological phases. The concept of quantum walk was proposed by Aharonov, Davidovich, and Zagury [125] and has been implemented in several experimental platforms, such as trapped atoms [126], trapped ions [127,128], optical fiber networks [129,130], and nuclear-magnetic resonance [131]. In quantum walks, the coin operator (also known as the "walker") acting on the internal degrees of freedom of particles replaces "coin flip", which introduces classical randomness by determining the particle trajectories in classical random walks. The dynamic evolution of quantum walk is determined by the Floquet operator U. The simplest version of quantum walk is the one-step evolution containing one coin operator and one conditional shift operator, as follows:

$$U = T \cdot R(\theta) \tag{27}$$

Here, the coin operator $R(\theta)$ is often chosen as a 2×2 matrix, which acts on the internal degrees of freedom. The conditional shift operator is often taken as follows:

$$T = \sum_x |x+1\rangle\langle x| \otimes |\uparrow\rangle\langle\uparrow| + |x-1\rangle\langle x| \otimes |\downarrow\rangle\langle\downarrow| \tag{28}$$

The conditional shift operator indicates the movement of the walker depending on its internal degrees of freedom. When treating one step evolution governed by U as the dynamics governed by the Hamiltonian, the effective Hamiltonian is presented as follows:

$$U = \exp(-iH_{\text{eff}}) \tag{29}$$

Therefore, the topology revealed in the quantum walk depends on the coin operator and can be resorted to the time-dependent effective Hamiltonian H_{eff}. By appropriately constructing U, the effective Hamiltonian H_{eff} can be made topologically non-trivial, resulting in topological phases in quantum walks [132,133]. These have been validated in experiments of discrete-time quantum walks [134–142], where U is applied to the walker at discrete time steps.

Consider a non-unitary Floquet operator U, the corresponding effective Hamiltonian H_{eff} is NH, and thus the NH phase can be studied. This idea was introduced by Rudner and Levitov in the NH–SSH model [143], realizing a passive version of PT-symmetric SSH chains where the average displacement of a particle is quantized and related to topological invariants. The experiment on non-unitary quantum walk reveals the existence of topological edge states at the domain walls of PT-symmetric SSH chains in optical setups with balanced gain and loss [144,145]. Wang et al. [146] observed skyrmions in a PT-symmetric non-unitary quantum walk; while Longhi [147] predicted the NH skin effect and symmetry breaking phase transition in a PT-symmetric discrete-time non-unitary quantum walk. A model with anisotropic hopping has also been achieved in a discrete-time non-unitary quantum walk, and the NH skin effect has been observed [147–159].

3.1.4. Mechanical System

The mechanical system provides another experimental platform for implementing the NH topology phase. There is a formal correspondence between Newton's second law and Schrödinger's equation, which can realize topological phases with phononic boundary states in mechanical systems. The topological phononic modes classified by Süsstrunk and Huber [160] appear at the boundaries of isostatic lattices built with springs [161], at boundaries of models composed of rotors and rigid beams [162], at dislocations in Kagome lattices composed of rigid disks [163], and as helical boundary states in devices composed of pendula [163]. When mass is replaced by a gyroscope, a gyroscopic metamaterial can be obtained, which has been shown to host acoustic boundary waves similar to edge states of the quantum Hall effect [164,165].

Similar to the method proposed by Kane and Lubensky [6] for studying isostatic lattices, a dynamical matrix associated with the lattice is written as $D = QQ^{\mathrm{T}}$, and the associated Hamiltonian matrix can be obtained by taking the square root, where Q and Q^{T} are its off-diagonal elements. One can conceive of the NH phononic phases. Starting from the general NH–Hamiltonian matrix with off-diagonal elements Q and $\widetilde{Q}$, the dynamical matrix is defined as $D = Q\widetilde{Q}$. The asymmetric $\left(D \neq D^{\mathrm{T}}\right)$ dynamical matrix of this NH–Hamiltonian $D = Q\widetilde{Q}$ has been experimentally implemented in robotic metamaterials by constructing a lattice consisting of mechanical rotors, control systems, and springs to combine robotics and active materials. In such a device, the NH skin effect in nonreciprocal realizations [166] and models similar to anisotropic SSH chains are demonstrated [167]. Schomerus [168] demonstrated through response theory that left eigenstates can also be detected in these devices; the right wave function specifies the response to external excitations, and the strength of response from the location of the disturbance is obtained by the left wave function. Based on this mechanism, when taking the response from the left and right wave functions into consideration, Schomerus [168] suggested that the skin effect is dependent on the phase transitions, and perturbations at the critical point for the phase transition lead to the divergence of sense. In this way, the biorthogonality of these non-Hermitian systems provides the results beyond the characteristic energy spectra. In addition, Brandenbourger et al. [166] and Ghatak et al. [167] studied the skin effect within experimentally elastic lattices when considering the feedback interactions in a non-local way.

The results provided by Rosa and Ruzzene [169] demonstrated that the bulk wave was able to be localized at various boundaries under the non-local control. In this way, corner localization can be formed through designed interactions. Scheibner et al. [170] demonstrated that an antisymmetric dynamical matrix $D = -D^{\mathrm{T}}$ can be constructed

with mechanical metamaterials. Odd elasticity was applied to realize non-conserving interactions. Furthermore, with the design of odd elasticity, bulk elastic waves can appear at the boundaries of one- and two-dimensional metamaterials [171], and host topological phase transitions. These phase transitions are modulated by the annihilation of active exceptional rings and gyroscope metamaterials [172]. Yoshida et al. [173] reported the realization of exceptional rings appear in mechanical metamaterials with friction.

In addition, phononic or acoustic materials [174] and metamaterials have been shown to host phononic edge states in microtubes [175], quantum spin Hall edge states in the form of elastic waves [176], and surface acoustic waves with negative refractive index on the surface of phononic Weyl semimetal [177]. Chiral edge states of quantum Hall effect can be implemented in a setup where acoustic waves propagate through rotating fluids arranged in crystals [178], and NH phase can be achieved through reasonable gain and loss. Shi et al. [179] implemented a PT-symmetric model where the gain is achieved through coherent acoustic sources, in which they obtain complete control over EPs and unidirectional transparency. Aurégan and Pagneux [180] also developed a PT-symmetric acoustic metamaterial in airflow ducts with gain and loss through the scattering of acoustic waves of diaphragm. Similarly, Rivet et al. [181] demonstrated that acoustic waves with constant pressure can exist in acoustic waveguides with gain and loss, while Zhu et al. [182] achieved EPs in lossy acoustic systems and demonstrated unidirectional propagation. Additional theories proposed to achieve PT symmetric second-order topological phases in acoustic metamaterials with gain and loss [183,184], as well as invisible acoustic sensors with PT symmetry [185]. In addition, more interesting topological phenomena based on acoustic materials have been reported and summarized [186–190].

3.2. Quantum Open Systems

In the above description, we reviewed the results of topological phases displayed on different classical platforms. However, there are some topological properties that cannot be fully demonstrated by classical systems. These properties are often related to the collective dynamics of multiple creation and annihilation operators, such as the topological properties of quantum open systems. In these quantum systems, there will be collective effects involving many creation and annihilation operators, such as the complicated couplings of quantum jump operators in quantum open systems, and so on [191–198].

3.2.1. The Lindblad Form in Quantum Open Systems

The introduction of non-Hermiticity in quantum many-body systems is the quantum dissipation caused by the coupling between the system and its environment. Experiments are usually conducted in the case of weak coupling between the system and a Markovian reservoir, where the Markovian reservoir is represented by the continuous electromagnetic field modes. In such situation, the evolution of the reduced density matrix ρ of an open system is described by the Lindblad master equation as follows:

$$\partial_t \rho = i[\rho, H] + \sum_n \left(L_n \rho L_n^\dagger - \frac{1}{2} \left\{ L_n^\dagger L_n, \rho \right\} \right), \tag{30}$$

where the jump operator L_n represents the coupling between the system and the environment. In order to intuitively understand the interplay between coherent quantum dynamics, dissipation, and topology in complex quantum many-body systems, the Lindblad equation can be written as $\partial_t \rho = i\left(\rho H_{\text{eff}}^\dagger - H_{\text{eff}} \rho\right) + \sum_n L_n \rho L_n^\dagger$, where the effective NH–Hamiltonian matrix is as follows:

$$H_{\text{eff}} = H - \frac{i}{2} \sum_n L_n^\dagger L_n, \tag{31}$$

which describes the dynamics of the system at short times [169]. At longer times, jump (or recycling) terms $\sum_n L_n \rho L_n^\dagger$ cannot be ignored, leading to decoherence (mixed states), while the effective non-Hermitian descriptions are constructed through less general pure states. Consider that the steady state of the Lindblad equation is identical to the $t \to \infty$

state governed by the non-unitary time evolution of the effective NH–Hamiltonian matrix. A simple and effective method to achieve this is to use $L_n|\Psi\rangle = 0$ to reverse engineer models [199], which selects the ground state $|\Psi\rangle$ of the Hamiltonian by using a suitable Lindblad jump operator. This method is particularly suitable for preparing topological phases, which have parent Hamiltonians composed of noncommutative terms that can be simultaneously minimized. It can serve as an effective method for utilizing dissipation and intuition from NH–Hamiltonian matrices to realize essentially Hermitian topological phases. For Gaussian systems described by the Lindblad equation, an effective NH description with damping matrix H_{D} can be systematically derived [200–202], which reflects different topological characteristics from the aforementioned effective NH [203]. Due to H_{D} determining how to suppress steady-state deviations, the long-time limit of the Lindblad equation is described. The non-Hermitian skin effect can be extended to the Lindblad case, and exceptional points can also occur within the Lindblad master equation framework.

The material junction in the quantum transport setup provides another possibility for realizing the NH topological phase and has been experimentally verified [203,204]. We now consider a setup where one side of the junction is considered a thermal reservoir (lead), which induces self-energy on the surface of system, resulting in an effective NH–Hamiltonian system $H_{\mathrm{NH}} = H + \sum_L^r(\omega)$, where H is the Hermitian–Hamiltonian matrix of the isolated system, $\sum_L^r(\omega)$ representing the self-energy close to the chemical potential field ω, reflecting the coupling between the system and the thermal reservoir. All eigenvalues of $\sum_L^r(\omega)$ satisfy $\mathrm{Im}[E] \leq 0$. Since $\sum_L^r(\omega)$ is usually non-Hermitian, it can have significant implications on the topology of interface states. This has been investigated in the superconducting junction with EPs [205–208], as well as in the interface between the topological insulator and the ferromagnetic leads [209,210]. In the latter case, the Hall conductance of the gapped phase loses its quantization [211,212], marking the destruction of the topology of the system that is well known from the Hermitian limit. However, the non-Hermiticity of this setup can also enhance topological properties; when the ferromagnet breaks the time reversal symmetry, it is predicted that it will typically open a gap. As shown by Bergholtz and Budich [213], there exists a critical magnetization angle beyond which dissipation overcomes the gap, thereby promoting the symmetry-protected surface topology to a nodal NH topology phase with EPs and NH–Fermi arcs that is independent of any symmetry.

NH topology may also occur in the boson Bogoliubov–de Gennes (BdG) problem. A general mapping between parameter-driven Hermitian bosonic models [211] and non-Hermitian–Hamiltonian models beyond BdG formalism can be used to implement NH topologically nontrivial models in Hermitian bosonic systems [212]. In addition, shaken cold atoms in optical lattices provide another platform for topological physics, and atomic losses can trigger the NH skin effect [213–219].

3.2.2. Emergent Dissipation in Closed Systems

Consider a quantum closed system that undergoes a unitary time evolution without dissipation. However, for interacting quantum many-body systems, their observables obey nonlinear equations of motion. Studies suggest that dissipation in the form of emergent non-Hermiticity can significantly affect the low-energy description of interacting and disordered quantum matter [220–226]. Similar to the concept of eigenstate thermalization [224,225], is a nonintegrable quantum system with a large number of degrees of freedom, which itself serves as a local observable thermal reservoir. In this situation, quasiparticles have a finite lifetime due to momentum scattering off each other or at impurities, the corresponding self-energy is non-Hermitian and can feature exceptional degeneracies and concomitant phenomena.

There have been studies proposing the emergent topological NH phenomena in heavy fermion systems, which are natural due to the extreme renormalization of bare electron properties [221]. Nodal semimetals are ideal systems for realizing NH Nodal phases [222,226–229]; strongly correlated Kondo materials [230] and magnons (spin-wave excitations of quantum magnets) are also ideal platforms for NH topology. Bosonic BdG also exists in magnons, providing an alternative way to achieve the NH phenomenon. In the early days [231,232], the idea of emergent EPs was also proposed early in nodal-line semimetals in the presence of external magnetic fields and radiated by circularly polarized light. Furthermore, the relationship between non-Hermiticity and superconductivity has been investigated at the level of a toy model [233].

4. Applications of Symmetry-Related Topological Phases in Quantum Information Processing

So far, we have reviewed topological phases under different symmetries and their implementations in various classical and quantum systems. However, topological properties are not only studied as a phenomenon, but as a means of controlling states to achieve efficient energy or information transmission. Among them, the use of exceptional points to achieve chiral topological control and transmission of energy can be viewed as a good application of topological properties.

4.1. Chiral Phenomenon of Dynamic Encircling Exceptional Points

In 1999, W.D. Heiss found that, in non-Hermitian systems with EPs, one can implement the exchange of two eigenstates when a circle of adiabatic evolution enclosing an EP happens using quasi-static dynamics [234]. In addition, when the Hamiltonian encircles EPs twice, the Berry phase is π. This phenomenon is different from the Hermitian system where, after encircling the diabolic point (DP), the eigenstate returns to itself and only obtains one geometric phase, namely the Berry phase. Studies suggest that the state flip caused by the so-called adiabatic encirclement of EPs is due to the self-orthogonal of the complex Riemann surface around EPs.

Uzdin et al. conducted further research [235] and found that when dynamically encircling the EPs, non-adiabatic phenomena may occur depending on the initial state. This property leads to asymmetric state flips and reflects a fundamental property of gain and loss systems; the adiabatic theorem does not apply to all eigenstates. As research deepens, it has been found that, in dynamic encirclement, the output state is predicted to be determined only by the rotational direction in the parameter space, independent of the input state. The chiral behavior is a manifestation of the destruction of the adiabatic theorem in non-Hermitian systems with gain and loss [236–238].

Figure 2 provides a more intuitive display of the differences in the results of encirclement evolution between Hermitian and non-Hermitian scenarios [239]. In Hermitian systems, the adiabatic theorem states that the topological properties of Hermitian systems originate from the Berry phase that they possess after a slowly encircling evolution in the parameter space. This phase is entirely determined by the geometric properties of the loop and, after the system undergoes the encircling evolution, the eigenstate remains unchanged except for the Berry phase, thus returning to the initial state (see Figure 2C,E). While in non-Hermitian systems, the above situation is changed. The symmetries in non-Hermitian systems, such as PT-symmetry, will lead to the existence of EPs in the system which, in turn, will result in the final state of the system when the dynamic encircling evolution is not identical to the initial state. Different chiral loops will lead to different final states. The loop no longer corresponds to a circular ring in Hermitian systems, but to a Riemannian surface similar to a Möbius ring (see Figure 2D,F), which is a manifestation of the typical topological properties in non-Hermitian systems.

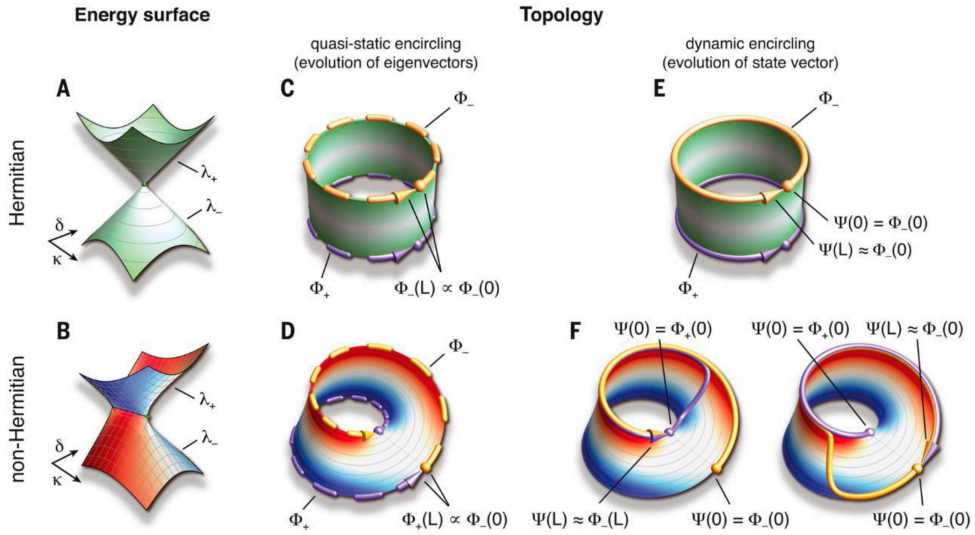

Figure 2. Different topological features corresponding to the encircling evolution of Hermitian and non-Hermitian systems [239]. (**A**) the energy surface of the Hermitian system. (**B**) the energy surface of the non-Hermitian system. (**C**,**D**) the qua-si-static encircling in the Hermitian and non-Hermitian systems. (**E**,**F**) the dynamic encircling in the Hermitian and non-Hermitian systems. Reproduced with permission [239] Copyright 2022, AAAS.

4.1.1. Implementation of Dynamic Encircling Exceptional Points in PT-Symmetry Systems

The PT symmetry in non-Hermitian systems leads to the existence of EPs. Although the topology of EPs have been experimentally explored [240,241], this chiral behavior has not been experimentally probed due to the difficulty in manipulation, since the phenomenon of the adiabatic destruction of dynamic encircling EPs was theoretically proposed in 2011. In 2016, Doppler et al. first implemented the process of dynamic encircling EPs through a dual-mode waveguide with appropriately designed boundaries and losses and observed the corresponding phenomenon [238]. They guided the incident wave to bypass the exception point and induce mode conversion during transmission, transforming the device into a powerful asymmetric switch between different waveguide modes. At the same time, H. Xu et al. also realized the same phenomenon in low-temperature optomechanical systems [237] and demonstrated the energy transfer between two vibration modes using topological operations. Due to the representativeness of waveguide systems, we will provide a detailed introduction to the experimental implementation in waveguide systems.

In the experimental scheme proposed by Jörg Doppler et al., an open system with two resonant modes coupled can be described by the following 2×2 non-Hermitian–Hamiltonian system:

$$H = \begin{pmatrix} \delta - i\gamma_1/2 & g \\ g & -i\gamma_2/2 \end{pmatrix} \tag{32}$$

Here g represents coupling, δ represents detuning, γ_1 and γ_2 are the loss rates of two modes, respectively. When $\delta = 0$, the Hamiltonian is PT-symmetric. Under specific parameter settings, such as $\delta = 0$ and $g = |\gamma_1 - \gamma_2|/4$, eigenvalues and eigenvectors will degenerate, which is the signature of EPs. In their design, the neighborhood at this point presents a self-orthogonal Riemann surface structure. EPs are located at the branching point where the Riemann surface splits. It is precisely this topology and gain-loss that allows us to bypass EPs, causing two eigenmodes to exchange or undergo non-adiabatic transitions back to themselves. This evolution requires continuously changing two system parameters along a closed path in the parameter space.

To observe the phenomena in practical systems, the Hamiltonian in Equation (32) is mapped to the microwave transmission problem of a smooth deformed metal waveguide with absorption. The waveguide is along the x-axis direction, and the following discussion is limited to a single transverse dimension y. Within this framework, the parameters encir-

cling of the 2 × 2 model shown above are transformed into slow variations by modulating along the periodic boundaries of the waveguide. At the EP, the Bloch wave number K and Bloch mode Λ of the electric field distribution $\varnothing(x,y) = \Lambda(x,y)e^{iKx}$ degenerate simultaneously. Furthermore, the harmonic solution $\varphi(x,y) = \varnothing(x,y,t)e^{-i\omega t}$ of the oscillating field with frequency ω follows the Helmholtz equation as follows:

$$\Delta\varnothing(x,y) + V(x,y)\varnothing(x,y) = 0 \tag{33}$$

Here Δ is the two-dimensional Laplace operator, $V(x,y) = \varepsilon(x,y)\frac{\omega^2}{c^2}$ is the complex potential proportional to the dielectric function ε, and c is the speed of light. For a straight rectangular waveguide with a fixed width of W in the y-direction, the solution of Equation (33) without dissipation is as follows:

$$\varnothing_n(x,y) = u_n(y)e^{ik_n x} \tag{34}$$

The transverse mode function is $u_n(y) = \sin(n\pi y/W)$ and the wave vector is $k_n = \sqrt{\omega^2/c^2 - n^2\pi^2/W^2}$. By selecting the suitable input frequency ω, the transmission problem can be naturally reduced to only two propagation modes $n = 1, 2$. To achieve controllable coupling between these modes, we consider a waveguide that is influenced by a boundary modulation $\xi(x) = \sigma\sin(k_b x)$. By selecting boundary wave numbers $k_b = k_1 - k_2 + \delta$ ($|\delta| \ll k_b$), near resonance scattering can appear between fundamentally different modes $\varnothing_1$ and $\varnothing_2$. The complete solution of the field can be written in the following form:

$$\varnothing(x,y) = \alpha_1(x)\varnothing_1(x,y) + \alpha_2(x)\varnothing_2(x,y) \tag{35}$$

The amplitude of a slowly changing mode is described as follows:

$$\psi(x,y) = \begin{pmatrix} c_1(x) \\ c_2(x) \end{pmatrix} = \begin{pmatrix} \sqrt{ik_1}\alpha_1(x) \\ \sqrt{-ik_2}\alpha_2(x) \end{pmatrix} e^{-i\delta x} \tag{36}$$

By using the Floquet Bloch hypothesis, a Schrödinger type equation can be obtained as follows:

$$i\partial_x \begin{pmatrix} c_1(x) \\ c_2(x) \end{pmatrix} = \begin{pmatrix} \delta(x) - i\gamma_1/2 & g(x) \\ g(x) & -i\gamma_2/2 \end{pmatrix} \begin{pmatrix} c_1(x) \\ c_2(x) \end{pmatrix}, \tag{37}$$

The slow variation of the parameters g and δ in Equation (32) can be achieved through the smooth variation of the potential field $V(x,y)$ in the waveguide. Through placing an absorbing material at the center of the waveguide can lead to losses due to the odd or even nature of $u_1(y)$ and $u_2(y)$. All parameters of the non-Hermitian–Hamiltonian system in Equation (32) can be determined in waveguide experiments. However, the Hamiltonian here is not used to describe temporal dynamics, but to describe longitudinal mode propagation. Therefore, the theoretical scheme of encircling EPs with time t corresponds to waveguide boundary parameters that slowly vary along the propagation direction x. Through the correspondence between the waveguide and the Hamiltonian, the phenomenon of encircling EPs can be observed in experiments.

Since the chiral phenomenon was experimentally verified, this field has attracted many attentions and made some important breakthroughs. For example, in 2018, Zhang et al. pointed out that the chirality of the dynamic encircling EPs in a ferromagnetic coupled waveguide actually depends on the starting point of the loop [242]. Especially, when the loop of dynamic encircling EPs starts from the PT-symmetric phase, the chiral behavior will disappear.

In 2021, Du's research group first realized the evolution of dynamic encircling EPs in a real quantum system, i.e., an atomic single spin structure, and also observed related phenomena [243].

4.1.2. Dynamic Encircling Exceptional Points in APT Symmetric Systems

The Hamiltonian system used in the waveguide experiments above satisfies PT-symmetry when one of its parameters is 0. The anti-parity–time- (APT)-symmetric system, whose Hamiltonian follows {PT, H} = 0, has recently attracted widespread attention [244–247]. Mathematically, the APT-symmetric Hamiltonian can be obtained by multiplying the PT-symmetric Hamiltonian with the imaginary number "*i*"; constructing a realistic APT-symmetric system is challenging as it requires the coupling between two states to be purely imaginary. Therefore, there are few experimental works on APT-symmetric systems. APT-symmetric systems also have EPs, but different Hamiltonians may lead to different physical phenomena. Therefore, it is very important to explore the unique features of APT-symmetric systems through experiments and apply them to new applications, especially those that cannot be achieved in traditional PT-symmetric systems. In 2019, Zhang et al. experimentally achieved the dynamic encircling of EPs in an APT-symmetric system [248], using the following Hamiltonian model:

$$H(t) = \begin{pmatrix} -g(t) + i\delta(t) & ik \\ ik & g(t) - i\delta(t) \end{pmatrix}, \tag{38}$$

where g and δ represent coupling and detuning, respectively. When $\delta = 0$, the Hamiltonian satisfied APT-symmetry $\{\mathrm{PT}, H\} = 0$. Subsequently, they utilized a waveguide platform to achieve dynamic encircling of electromagnetic pulses. The experimental platform consists of three waveguides with an absorber in the middle. As shown in Figure 3, the distance between the two gaps continuously changes along the waveguide, making the transmission of electromagnetic waves through the system equivalent to a loop encircling EPs in the parameter space. Research has found that chiral transmission behavior occurs when the starting/ending point is located in the PT-broken phase, where the eigenmode is a symmetry-broken mode. This is opposite to PT-symmetric systems, where chiral behavior only applies to symmetric and anti-symmetric modes. The discovery of new physics in APT-symmetric systems can lead to new applications, where symmetry-broken modes can be used for asymmetric mode switching, which cannot be implemented using PT-symmetric systems.

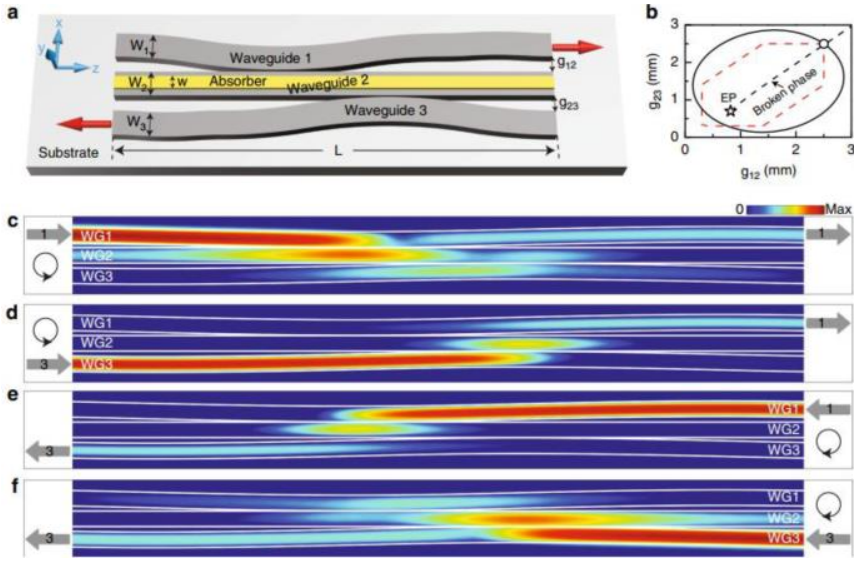

Figure 3. Chiral mode switch in an APT-symmetric coupled waveguide system [248]. (**a**) the structure of system; (**b**) the circling tra-jectory around the EP; (**c**–**f**) the evolution results from different inputs and encircling directions. Figures are adapted from CC-BY open access publications Springer Nature.

4.1.3. Study on the Efficiency of Chiral Transmission

The efficiencies of chiral transmissions in the experiments introduced in Sections 4.1.1 and 4.1.2 are quite low, mainly because the path related losses generated by slowly encircling along a continuous loop around EPs. Due to this inherent low efficiency, chiral transmission and other non-Hermitian phenomena are still out of reach for technological applications. The implementation of practical non-Hermitian photonic devices and systems requires a protocol of encircling EPs that can achieve high transmission efficiency.

In order to reduce the length of waveguide and improve transmission efficiency, the encircling loop should be reduced while ensuring the parameter evolute adiabatically. However, if EPs remain fixed in the parameter space, shrinking the loop may be impossible because the EPs may be excluded from the loop. In 2022, Liu et al. designed and fabricated a non-Hermitian waveguide system based on subwavelength gratings (SWGs) to demonstrate the mobile electromagnetic pulses in a system [249]. The parameters can be adiabatically evolved along a smaller loop through a moving EP, which can significantly reduce the losses compared to fixed EPs, and the mode transparency has significantly improved. This method of encircling moving EPs has great potential for reducing the path, such as in highly integrated broadband optical switches and converters for telecommunications wavelength operation.

In 2020, Chen's group proposed a new protocol of encircling EPs to overcome the challenge of low transmission efficiency [250]. The protocol utilizes rapid variations of a Hamiltonian at the parameter boundaries, known as "Hamiltonian hopping", which enables robust chiral mode switching with near unity efficiency. When the parameters of the system approach infinity, the eigenstates of the Hamiltonian converge, and by transitioning between these states, chiral dynamics related to the EP can be obtained without path dependent loss. By mapping the required Hamiltonian parameters onto appropriately designed coupled waveguides, chiral mode switching was theoretically predicted and experimentally demonstrated on a standard silicon-insulator platform. Research has shown that the proposed protocol can realize almost uniform transmission efficiency across the entire telecommunications spectrum due to its robustness to the encircling path and has demonstrated an efficiency near 90% in experiments at a wavelength of 1550 nm.

4.2. Topological Transmission of Quantum Entangled States

The development of quantum technology has received widespread attention in recent years. One important research objective is to achieve efficient and stable quantum information transmission and processing. Compared with classical information transmission, quantum information transmission can achieve absolute security; the speed of quantum information processing can be improved by orders of magnitude. Although the transmission and processing of quantum information have many advantages, the quantum states storing quantum information are very "fragile" and are easily affected by the surrounding environment, which greatly limits the subsequent transmission and processing of quantum information. Therefore, achieving stable quantum information transmission and processing in real physical systems has become a hot topic of concern for everyone. Due to the strong robustness of topologically protected boundary states to local disturbances, they can be utilized for quantum state processing.

Recently, the application of topological protection in quantum entanglement transmission has also attracted wide attention. In 2018, Andrea Blanco-Redondo et al. used a nanophotonic experimental platform to achieve topological protection of two-photon states [251]. Their experiment was based on a one-dimensional silicon nanowire array with alternating adjustable length and gaps, which can be used to adjust the coupling strength between adjacent nanowires and form an SSH lattice. The defects between the strong couplings of the lattice act as topological interfaces in the SSH lattice model and generate topological edge states at the interface between the two phases. Two photons are transmitted at this topological interface and have been proven to have robust spatial modes against disorder.

Based on the above platform, the team successfully achieved the first experimental proof of topological protection for entangled two-photon states of spatial modes in 2019 [252]. Figure 4 shows a scanning electron microscope (SEM) image of a fabricated lattice, in which two topological defects between long couplings are separated by five dimers, i.e., ten nanowires, to avoid coupling between the two topological defect modes. The parameters of the silicon nanowires contained in the lattice in the experiment are length $l = 381$ um, height $h = 220$ nm, and width $w = 450$ nm. The gaps separating the waveguides alternate between short gaps $g_s = 173$ nm and long gaps $g_l = 307$ nm. Entangled two-photon states are generated through spontaneous four-wave mixing (SFWM) inside the photonic chip. At the input of the chip, a mode-locked laser is used to emit 1550 nm picosecond pulses, which are divided into two arms with equal intensity using a multimode interferometer. Then point each arm towards the central waveguide in two defects between strong couplings to excite the two topological modes of the lattice. When short pulses propagate through silicon nanowires, the high peak power and spatial limitations of light result in the probabilistic generation of correlated signal and idle photon pairs over a wide frequency range through SFWM. These frequency dependent photon pairs generate spatial entanglement. At the output of the lattice, they filter signal photons and idle photons that satisfy energy conservation at 1545 nm and 1555 nm and detect them separately using superconducting nanowire single-photon detectors (SSPDs). By measuring the matching arrival time of the signal and idle photon pairs through a time-correlated circuit (TCC), the spatial contour of the entangled two-photon state can be drawn. Finally, they demonstrated that topological structures can indeed protect entanglement from the effects of disorder and defects by intentionally introducing varying degrees of disorder at waveguide positions.

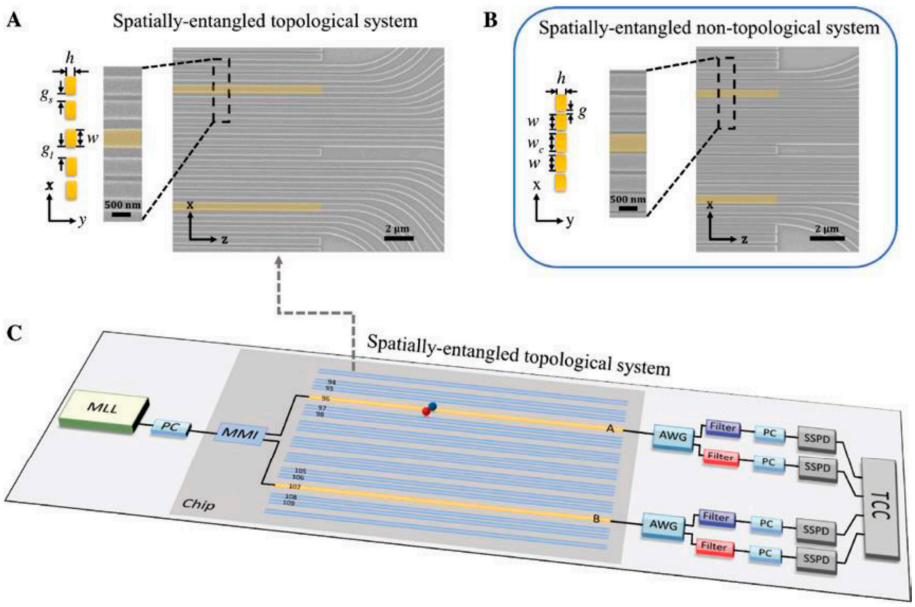

Figure 4. Nanophotonic experimental platform for entanglement transmission with topological protection [252]. (**A**,**B**) the topological and non-topological systems. (**C**) the whole experimental process for the entanglement transmission. Figures are adapted from CC-BY open access publications De Gruyter.

In 2019, Jin's group realized topologically protected two-photon quantum correlation transmission [253]. In the experiment, they used the direct writing technology of a femtosecond laser to fabricate photonic chips. By creating a non-diagonal Harper lattice model in borosilicate glass, the model inherited the robust boundary state of a two-dimensional integer quantum Hall effect and had similar topological features. As shown on the left side of Figure 5, when the two-photon state evolves in the topological photonic lattice on the photonic chip, and when the photon is incident from the middle of the chip, i.e., the non-

topological area, it can be observed that the scattering loss is significant. However, when incidents from the boundary, due to topological protection, the two-photon at the boundary is highly likely to be localized at the boundary, preventing scattering loss problems. In the experiment, they placed the photonic chip with above features in the experimental setup shown on the right side of Figure 5, a periodically polarized potassium titanyl phosphate (PPKTP) crystal generated both horizontally polarized photons and vertically polarized photons with a wavelength of 810.4 nm through a spontaneous parameter down conversion. After the designed polarization rotation and projection, both are converted to horizontal polarization with a 25% probability. Then they are injected simultaneously into the lattice of the photonic chip. Here, the single-photon sensitive enhanced CCD (ICCD) camera probes the emission distribution of photons, and the avalanche photodiode (APD) detects the quantum correlation of photon pairs after the fiber splitter. Finally, they obtained a violation of the Cauchy–Schwarz inequality with high cross-correlation and up to 30 standard deviations by analyzing the quantum correlation of photons starting from topologically nontrivial boundary states. Moreover, they prepared different quantum sources and experimentally demonstrated the robustness of topological protection to wavelength differences and the distinguishability of two photons. Subsequently, based on the above research, the group implemented the topological protection of two-photon polarization entangled states on photonic chips in 2022 [219]. In the experiment, they utilized laser direct writing technology to realize the topological lattice of the SSH model on a photonic chip. BBO crystals were utilized to generate polarized entangled photon pairs, where one photon is directly received by the detector and the other photon is incident on the photonic chip for coincidence measurement, as shown in Figure 6. Due to the existence of topological protection, the entangled state maintains high concurrency and purity during transmission. The output entangled states of photonic lattices with transmission distances of z = 20 mm and 140 mm were measured, and the corresponding entanglement degrees were 0.88 $\pm$ 0.02 and 0.95 $\pm$ 0.02, respectively, while the purities were 0.89 $\pm$ 0.02 and 0.94 $\pm$ 0.03, respectively. However, it can be seen from the density matrix that the fidelity of the entangled state cannot be maintained continuously during transmission but varies greatly. This problem also urgently needs to be solved.

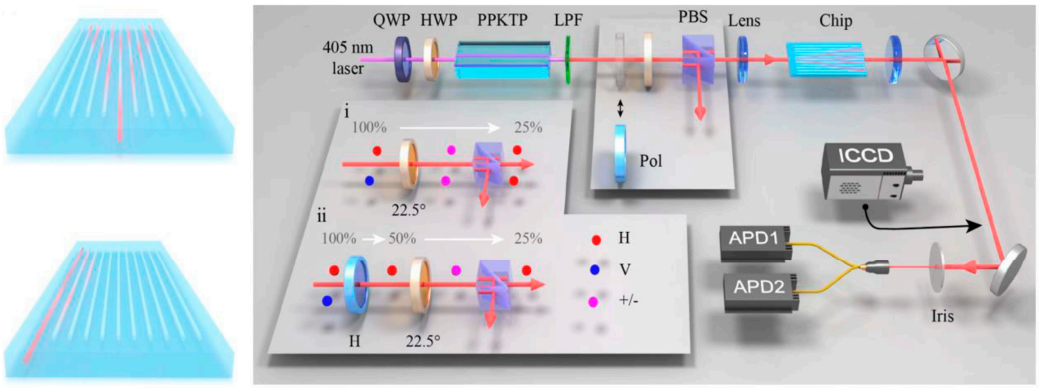

Figure 5. Experimental schematic diagram of implementing topological protection for two-photon quantum correlation [253]. Figures are adapted from CC-BY open access publications Optica Publishing Group.

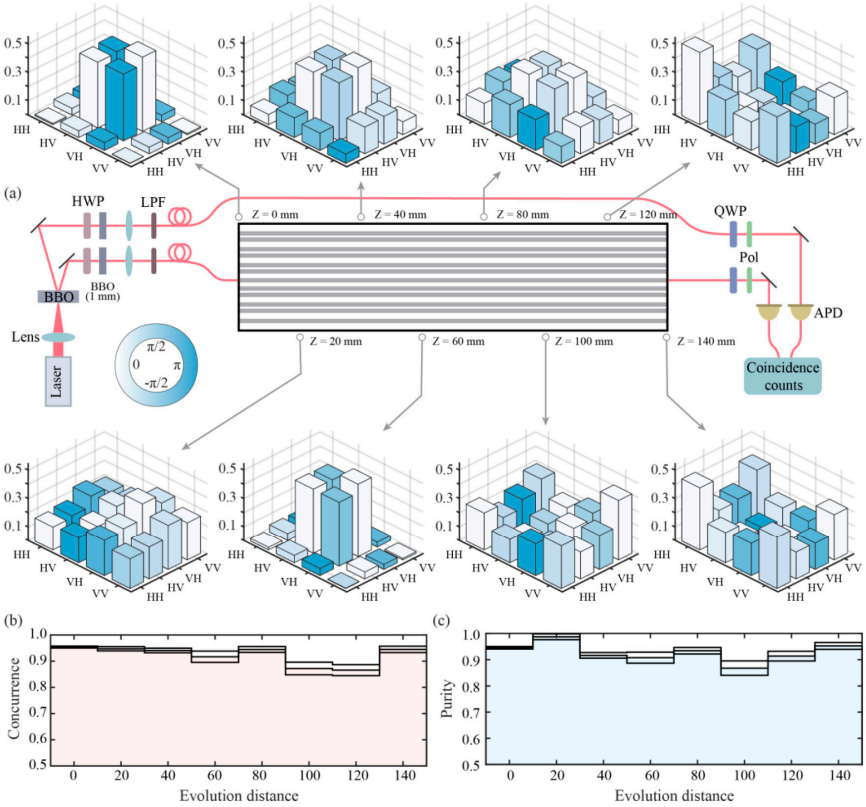

Figure 6. Schematic diagram and results of the experiment on topologically protected two-photon polarization entangled state transmission [254]. (**a**) the obtained density matrices at different positions during the transmission. (**b**,**c**) the con-currence and fidelity at different positions. Figures are adapted from CC-BY open access publications Elsevier.

Zhang's group constructed a special type of topological channel using an anti-design method, effectively solving the problem that the fidelity of quantum entangled state transmission rapidly decreases with transmission distance [255–258]. In the topological channel they designed, quantum entangled states can maintain high fidelity suffering transmission or conversion, and the idea has been verified in experiments based on a photonic quantum walk platform. As shown in Figure 7a–d, they incident the two-photon maximum entangled state into the constructed topological channel. At each step of quantum walk, the angle at which the photon passes through the half slide is determined through anti-design. Compared with directly transmitting entangled states in a topological channel without an anti-design, the topological channel designed in this way can provide a sufficiently high localization probability and extremely high fidelity for the quantum entangled states transmitted in the topological channel, as shown in Figure 7e. Furthermore, they also introduced the corresponding approach of an anti-design topological channel into the entangled state conversion. After the anti-design, the topological channel can maintain a high probability of localization during the process of entangled state conversion. The transformed entangled state also has extremely high fidelity, as shown in Figure 7f. The relevant results not only provide new ideas for optical quantum information processing, but offer excellent application scenarios for the study of topological photonics.

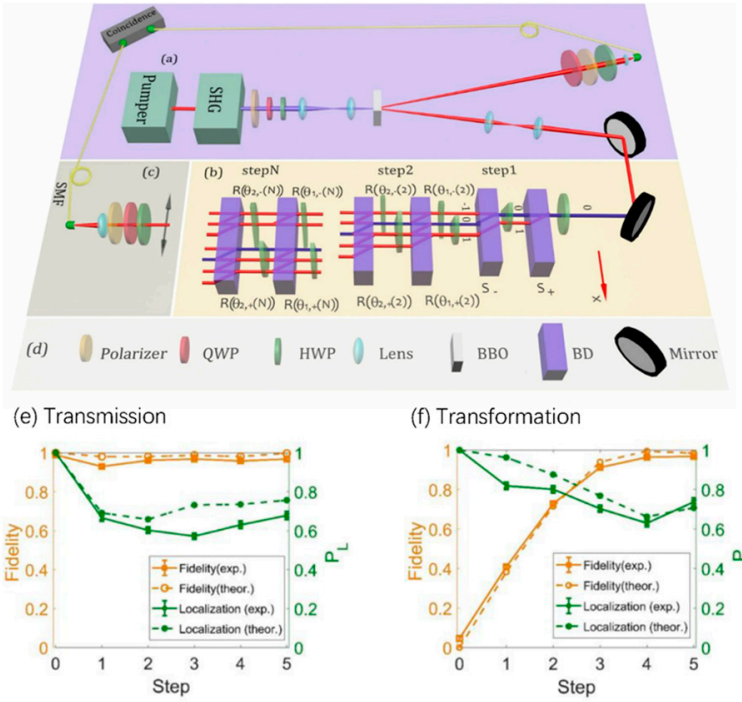

Figure 7. (**a**) Preparation of Two-Photon Entangled States. (**b**) Multi-step quantum random walk. The quantum random walk of each step consists of a translation operator (S_+ and S_-) and a coin operator ($R(\theta_1)$ and $R(\theta_2)$), $U_{walk,i} = S_- R(\theta_{2,\pm}(i)) S_+ R(\theta_{1,\pm}(i))$. The blue solid line marks the location of the topological channel. (**c**) The final state by coincidence measurement. (**d**) List of components. (**e**) The perfect transmission of entangled states $|\varnothing_1\rangle = \frac{1}{\sqrt{2}}(|00\rangle + |11\rangle)$. Even after 5 steps, there is still a high fidelity (above 98%, brown line) and a high localization probability (green line); (**f**) The perfect conversion of entangled states ($|\varnothing_1\rangle = \frac{1}{\sqrt{2}}(|00\rangle + |11\rangle) \rightarrow |\varnothing_4\rangle = \frac{1}{\sqrt{2}}(|01\rangle - |10\rangle)$); After 4 steps, the fidelity between the output states $|\varnothing_4\rangle$ is extremely high (above 99%, brown line), and the localization probability is also high (green line) [255]. Reproduced with permission [255] Copyright 2022, Wiley Online Library.

Furthermore, the research group designed a non-Hermitian quantum walk and achieved efficiently topological control on quantum states. The research group studied the phenomenon of quantum state transition encircling exceptional points and exceptional lines both in theory and experiment based on a non-Hermitian quantum walk platform. Compared with the case of encircling exceptional points, it was found that the final state of the evolution encircling exceptional line is independent of the initial state and evolution direction, and the transfer of quantum states is more efficient. Moreover, the group has developed a robust method for entangled state generation that is insensitive to the incident state and has been experimentally verified [257]. Furthermore, an effective solution is provided for realizing high fidelity and stable operation of quantum entangled states by designing fourth-order degenerate exceptional points and realized topologically protected entangled state chiral switches. Due to the fact that the designed Riemann energy surface with degenerate exceptional points shares the same eigenstates with entangled states, asymmetric transformations between entangled states can be achieved by encircling exceptional points. Due to the topological properties of the Riemann surface, the manipulation of entangled states is topologically protected. In addition, these phenomena have been experimentally demonstrated through the construction of a quantum walk platform [258].

5. Conclusions and Outlook

In this review, we start with symmetry and analyze the topological phases that will form under different symmetries, as well as the topological properties. When considering chiral symmetry, time-reversal symmetry, and particle-hole symmetry, ten different

topological phases will form in Hermitian systems; When other symmetries, such as mirror symmetry, are introduced, more topological phases will be formed. In addition, in non-Hermitian systems, due to the differences between the transpose operation and the Hermitian conjugation operation, more topological phases will also be formed. Next, we reviewed the observation of topological phases on different experimental platforms and the topological phenomena unique to quantum systems. Then, for the application of topological phases, we conducted a detailed exploration using chiral energy transfer as an example and reviewed the research on the application of chiral topological modulation to the quantum information processing.

Current research on topological properties is no longer limited to topological phases related to symmetry. Currently, research on topological phases related to asymmetry has also received great attention, such as topological phase transitions caused by dislocations and tailored structures [259–261]. The research on many-body systems and open systems is also developing, such as the skin effect generated in many-body systems and the phase transitions related to measurement and feedback generated in quantum open systems [262–266]. In particular, the observation of chiral topological dynamics has been realized on a digital quantum computation, which combines the advances of quantum computation and topology [262,263].

The use of topological phenomena in non-Hermitian physics to achieve topological protection of entangled states has been a focus of research in recent years, as it provides a feasible path for the practical application of quantum entanglement as an important resource. However, due to the complexity of the work, it is also highly challenging. Therefore, as an emerging and important direction, there are still many issues that need to be addressed. Here, we provide a brief summary of the prospects for future work:

Firstly, current work utilizing non-Hermitian topological phenomena mainly focuses on manipulating Bell states, while there has been no progress in research related to higher dimensional entanglements, such as GHZ states. To address this issue, it can be achieved by increasing the dimensionality of the studied system, but it also requires topological phenomena in high-dimensional non-Hermitian systems as a basis. Therefore, utilizing high-dimensional quantum walk models to study and discover new high-dimensional topological phenomena, and extending to the application of GHZ states, is a highly worthwhile direction for research.

Secondly, it is very hard to realize photon coupling in free space, but in waveguide systems on integrated chips, photon coupling can be effectively achieved by adjusting the distance between adjacent waveguides, and the non-unitary evolution of entangled states on integrated chips is much easier to achieve. Therefore, it is also necessary to combine non-Hermitian topological theory with integrated chip systems and further expand it [267–269].

Author Contributions: Conceptualization, R.Z. and T.C.; validation, R.Z. and T.C.; formal analysis, R.Z.; investigation, T.C.; data curation, R.Z. and T.C.; writing—original draft preparation, R.Z.; writing—review and editing, T.C.; supervision, T.C.; project administration, R.Z. and T.C.; funding acquisition, T.C. All authors have read and agreed to the published version of the manuscript.

Funding: This research was funded by National Natural Science Foundation of China grant numbers 12374323 and 11974046.

Data Availability Statement: Data are contained within the article.

Conflicts of Interest: The authors declare no conflict of interest.

References

1. Verbaarschot, J. Spectrum of the QCD Dirac operator and chiral random matrix theory. *Phys. Rev. Lett.* **1994**, *72*, 2531. [CrossRef] [PubMed]
2. Foster, M.S.; Ludwig, A.W.W. Metal-insulator transition from combined disorder and interaction effects in Hubbard-like electronic lattice models with random hopping. *Phys. Rev. B* **2008**, *77*, 165108. [CrossRef]
3. Dyson, F.J. The Dynamics of a Disordered Linear Chain. *Phys. Rev.* **1953**, *92*, 1331. [CrossRef]

4. Gurarie, V.; Chalker, J.T. Some Generic Aspects of Bosonic Excitations in Disordered Systems. *Phys. Rev. Lett.* **2002**, *89*, 136801. [CrossRef]
5. Gurarie, V.; Chalker, J.T. Bosonic excitations in random media. *Phys. Rev. B* **2003**, *68*, 134207. [CrossRef]
6. Broedersz, C.; Mao, X.; Lubensky, T.C.; MacKintosh, F.C. Criticality and isostaticity in fibre networks. *Nat. Phys.* **2011**, *7*, 983. [CrossRef]
7. Turner, A.M.; Zhang, Y.; Vishwanath, A. Entanglement and inversion symmetry in topological insulators. *Phys. Rev. B* **2010**, *82*, 241102. [CrossRef]
8. Hughes, T.L.; Prodan, E.; Bernevig, B.A. Inversion-symmetric topological insulators. *Phys. Rev. B* **2011**, *83*, 245132. [CrossRef]
9. Chang, P.-Y.; Mudry, C.; Ryu, S. Symmetry-protected entangling boundary zero modes in crystalline topological insulators. *J. Stat. Mech.* **2014**, *2014*, P09014. [CrossRef]
10. Kennedy, R.; Zirnbauer, M.R. Bott Periodicity for Z2 Symmetric Ground States of Gapped Free-Fermion Systems. *Commun. Math. Phys.* **2016**, *342*, 909. [CrossRef]
11. Zirnbauer, M.R. Riemannian symmetric superspaces and their origin in random-matrix theory. *J. Math. Phys.* **1996**, *37*, 4986. [CrossRef]
12. Altland, A.; Zirnbauer, M.R. Nonstandard symmetry classes in mesoscopic normal-superconducting hybrid structures. *Phys. Rev. B* **1997**, *55*, 1142. [CrossRef]
13. Chiu, C.-K.; Teo, J.C.Y.; Schnyder, A.P.; Ryu, S. Classification of topological quantum matter with symmetries. *Rev. Mod. Phys.* **2016**, *88*, 035005. [CrossRef]
14. Schnyder, A.P.; Ryu, S.; Furusaki, A.; Ludwig, A.W.W. Classification of topological insulators and superconductors in three spatial dimensions. *Phys. Rev. B* **2008**, *78*, 195125. [CrossRef]
15. Kitaev, A. Periodic table for topological insulators and superconductors. *AIP Conf. Proc.* **2009**, *1134*, 22–30.
16. Ryu, S.; Schnyder, A.P.; Furusaki, A.; Ludwig, A.W.W. Topological insulators and superconductors tenfold way and dimensional hierarchy. *New J. Phys.* **2010**, *12*, 065010. [CrossRef]
17. Benalcazar, W.A.; Bernevig, B.A.; Hughes, T.L. Quantized electric multipole insulators. *Science* **2017**, *357*, 61. [CrossRef]
18. Kawabata, K.; Shiozaki, K.; Ueda, M.; Sato, M. Symmetry and Topology in Non-Hermitian Physics. *Phys. Rev. X* **2019**, *9*, 041015. [CrossRef]
19. Zhou, H.; Lee, J.Y. Periodic table for topological bands with non-Hermitian symmetries. *Phys. Rev. B* **2019**, *99*, 235112. [CrossRef]
20. Ashida, Y.; Gong, Z.; Ueda, M. Non-Hermitian Physics. *Adv. Phys.* **2020**, *69*, 249–435. [CrossRef]
21. Esaki, K.; Sato, M.; Hasebe, K.; Kohmoto, M. Edge states and topological phases in non-Hermitian systems. *Phys. Rev. B* **2011**, *84*, 205128. [CrossRef]
22. Lee, J.Y.; Ahn, J.; Zhou, H.; Vishwanath, A. Topological Correspondence between Hermitian and Non-Hermitian Systems: Anomalous Dynamics. *Phys. Rev. Lett.* **2019**, *123*, 206404. [CrossRef] [PubMed]
23. Bessho, T.; Sato, M. Nielsen-Ninomiya Theorem with Bulk Topology: Duality in Floquet and Non-Hermitian Systems. *Phys. Rev. Lett.* **2021**, *127*, 196404. [CrossRef]
24. Hŏrava, P. Stability of Fermi Surfaces and *K* Theory. *Phys. Rev. Lett.* **2005**, *95*, 016405. [CrossRef]
25. Matsuura, S.; Chang, P.Y.; Schnyder, A.P.; Ryu, S. Protected boundary states in gapless topological phases. *New J. Phys.* **2013**, *15*, 065001. [CrossRef]
26. Zhao, Y.X.; Wang, Z.D. Topological Classification and Stability of Fermi Surfaces. *Phys. Rev. Lett.* **2013**, *110*, 240404. [CrossRef]
27. Zhao, Y.X.; Wang, Z.D. Topological connection between the stability of Fermi surfaces and topological insulators and superconductors. *Phys. Rev. B* **2014**, *89*, 075111. [CrossRef]
28. Zhao, Y.X.; Schnyder, A.P.; Wang, Z.D. Unified Theory of *PT* and *CP* Invariant Topological Metals and Nodal Superconductors. *Phys. Rev. Lett.* **2016**, *116*, 156402. [CrossRef]
29. Zhao, Y.X.; Lu, Y. *PT*-Symmetric Real Dirac Fermions and Semimetals. *Phys. Rev. Lett.* **2017**, *118*, 056401. [CrossRef]
30. Morimoto, T.; Furusaki, A. Weyl and Dirac semimetals with $\mathbb{Z}2$ topological charge. *Phys. Rev. B* **2014**, *89*, 235127. [CrossRef]
31. Kobayashi, S.; Shiozaki, K.; Tanaka, Y.; Sato, M. Topological Blount's theorem of odd-parity superconductors. *Phys. Rev. B* **2014**, *90*, 024516. [CrossRef]
32. Shiozaki, K.; Sato, M. Topology of crystalline insulators and superconductors. *Phys. Rev. B* **2014**, *90*, 165114. [CrossRef]
33. Chiu, C.K.; Schnyder, A.P. Classification of reflection-symmetry-protected topological semimetals and nodal superconductors. *Phys. Rev. B* **2014**, *90*, 205136. [CrossRef]
34. Kawabata, K.; Bessho, T.; Sato, M. Classification of Exceptional Points and Non-Hermitian Topological Semimetals. *Phys. Rev. Lett.* **2019**, *123*, 066405. [CrossRef]
35. Kato, T. Perturbation Theory for Linear Operators. In *Classics in Mathematics*; Springer Science & Business Media: Berlin, Germany, 2013; Volume 132.
36. Berry, M.V. Physics of Nonhermitian Degeneracies. *Czechoslov. J. Phys.* **2004**, *54*, 1039–1047. [CrossRef]
37. Heiss, W. The physics of exceptional points. *J. Phys. A Math. Theor.* **2012**, *45*, 444016. [CrossRef]
38. Shen, H.; Zhen, B.; Fu, L. Topological Band Theory for Non-Hermitian Hamiltonians. *Phys. Rev. Lett.* **2018**, *120*, 146402. [CrossRef]
39. Kozii, V.; Fu, L. Non-Hermitian topological theory of finite-lifetime quasiparticles: Prediction of bulk Fermi arc due to exceptional point. *arXiv* **2017**, arXiv:1708.05841. [CrossRef]

40. Zhou, H.; Peng, C.; Yoon, Y.; Hsu, C.W.; Nelson, K.A.; Joannopoulos, J.D.; Soljačić, M.; Zhen, B. Observation of bulk Fermi arc and polarization half charge from paired exceptional points. *Science* **2018**, *359*, 1009. [CrossRef]
41. Papaj, M.; Isobe, H.; Fu, L. Nodal arc of disordered Dirac fermions and non-Hermitian band theory. *Phys. Rev. B* **2019**, *99*, 201107. [CrossRef]
42. Bergholtz, E.J.; Budich, J.C.; Kunst, F.K. Exceptional topology of non-Hermitian systems. *Rev. Mod. Phys.* **2021**, *93*, 015005. [CrossRef]
43. Zhou, H.; Lee, J.Y.; Liu, S.; Zhen, B. Exceptional surfaces in PT -symmetric non-Hermitian photonic systems. *Optica* **2019**, *6*, 190. [CrossRef]
44. Zyuzin, A.A.; Zyuzin, A.Y. Flat band in disorder-driven non-Hermitian Weyl semimetals. *Phys. Rev. B* **2018**, *97*, 041203(R). [CrossRef]
45. Yoshida, T.; Peters, R.; Kawakami, N. Non-Hermitian perspective of the band structure in heavy-fermion systems. *Phys. Rev. B* **2018**, *98*, 035141. [CrossRef]
46. Yoshida, T.; Peters, R.; Kawakami, N.; Hatsugai, Y. Symmetry-protected exceptional rings in two-dimensional correlated systems with chiral symmetry. *Phys. Rev. B* **2019**, *99*, 121101(R). [CrossRef]
47. Bergholtz, E.J.; Budich, J.C. Non-Hermitian Weyl physics in topological insulator ferromagnet junctions. *Phys. Rev. Res.* **2019**, *1*, 012003(R). [CrossRef]
48. Kimura, K.; Yoshida, T.; Kawakami, N. Chiral-symmetry protected exceptional torus in correlated nodal-line semimetals. *Phys. Rev. B* **2019**, *100*, 115124. [CrossRef]
49. Zhen, B.; Hsu, C.W.; Igarashi, Y.; Lu, L.; Kaminer, I.; Pick, A.; Chua, S.L.; Joannopoulos, J.D.; Soljačić, M. Spawning rings of exceptional points out of Dirac cones. *Nature* **2015**, *525*, 354. [CrossRef]
50. Xu, Y.; Wang, S.T.; Duan, L.M. Weyl Exceptional Rings in a Three-Dimensional Dissipative Cold Atomic Gas. *Phys. Rev. Lett.* **2017**, *118*, 045701. [CrossRef]
51. Okugawa, R.; Yokoyama, T. Topological exceptional surfaces in non-Hermitian systems with parity-time and parity-particle-hole symmetries. *Phys. Rev. B* **2019**, *99*, 041202(R). [CrossRef]
52. Budich, J.C.; Carlström, J.; Kunst, F.K.; Bergholtz, E.J. Symmetry-protected nodal phases in non-Hermitian systems. *Phys. Rev. B* **2019**, *99*, 041406(R). [CrossRef]
53. Cerjan, A.; Huang, S.; Chen, K.P.; Chong, Y.; Rechtsman, M.C. Experimental realization of a Weyl exceptional ring. *Nat. Photon.* **2019**, *13*, 623. [CrossRef]
54. Okuma, N.; Sato, M. Non-Hermitian Topological Phenomena A Review. *Annu. Rev. Condens. Matter Phys.* **2023**, *14*, 83–107. [CrossRef]
55. Haldane, F.D.M.; Raghu, S. Possible Realization of Directional Optical Waveguides in Photonic Crystals with Broken Time-Reversal Symmetry. *Phys. Rev. Lett.* **2008**, *100*, 013904. [CrossRef]
56. Raghu, S.; Haldane, F.D.M. Analogs of quantum-Halleffect edge states in photonic crystals. *Phys. Rev. A* **2008**, *78*, 033834. [CrossRef]
57. Ozawa, T.; Price, H.; Amo, A.; Goldman, N.; Hafezi, M.; Lu, L.; Rechtsman, M.; Schuster, D.; Simon, J.; Zillberberg, O.; et al. Topological photonics. *Rev. Mod. Phys.* **2019**, *91*, 015006. [CrossRef]
58. Albert, V.V.; Glazman, L.I.; Jiang, L. Topological Properties of Linear Circuit Lattices. *Phys. Rev. Lett.* **2015**, *114*, 173902. [CrossRef]
59. Ningyuan, J.; Owens, C.; Sommer, A.; Schuster, D.; Simon, J. Time- and Site-Resolved Dynamics in a Topological Circuit. *Phys. Rev. X* **2015**, *5*, 021031. [CrossRef]
60. Lee, C.H.; Imhof, S.; Berger, C.; Bayer, F.; Brehm, J.; Molenkamp, L.W.; Kiessling, T.; Thomale, R. Topolectrical circuits. *Commun. Phys.* **2018**, *1*, 39. [CrossRef]
61. Mao, X.M.; Lubensky, T.C. Coherent potential approximation of random nearly isostatic kagome lattice. *Phys. Rev. E* **2011**, *83*, 011111. [CrossRef]
62. Huber, S.D. Topological mechanics. *Nat. Phys.* **2016**, *12*, 621–623. [CrossRef]
63. Wang, Z.; Chong, Y.D.; Joannopoulos, J.D.; Soljačić, M. Reflection-Free One-Way Edge Modes in a Gyromagnetic Photonic Crystal. *Phys. Rev. Lett.* **2008**, *100*, 013905. [CrossRef] [PubMed]
64. Lu, L.; Fu, L.; Joannopoulos, J.D.; Soljacic, M. Weyl points and line nodes in gyroid photonic crystals. *Nat. Photonics* **2013**, *7*, 294–299. [CrossRef]
65. Midya, B.; Zhao, H.; Feng, L. Non-Hermitian photonics promises exceptional topology of light. *Nat. Commun.* **2018**, *9*, 2674. [CrossRef]
66. Feng, L.; Xu, Y.L.; Fegadolli, W.S.; Lu, M.H.; Oliveira, J.E.B.; Almeida, V.R.; Chen, Y.F.; Scherer, A. Experimental demonstration of a unidirectional reflectionless parity-time metamaterial at optical frequencies. *Nat. Mater.* **2013**, *12*, 108–113. [CrossRef]
67. Kulishov, M.; Laniel, J.M.; B'elanger, N.; Azaña, J.; Plant, D.V. Nonreciprocal waveguide Bragg gratings. *Opt. Express* **2005**, *13*, 3068. [CrossRef]
68. Lin, Z.; Ramezani, H.; Eichelkraut, T.; Kottos, T.; Cao, H.; Christodoulides, D.N. Unidirectional Invisibility Induced by PT—Symmetric Periodic Structures. *Phys. Rev. Lett.* **2011**, *106*, 213901. [CrossRef]
69. Longhi, S. Invisibility in PT-symmetric complex crystals. *J. Phys. A* **2011**, *44*, 485302. [CrossRef]
70. Jones, H.F. Analytic results for a PT-symmetric optical structure. *J. Phys. A* **2012**, *45*, 135306. [CrossRef]

71. Bliokh, K.Y.; Leykam, D.; Lein, M.; Nori, F. Topological non-Hermitian origin of surface Maxwell waves. *Nat. Commun.* **2019**, *10*, 580. [CrossRef]
72. Peng, B.; Özdemir, K.; Lei, F.; Monifi, F.; Gianfreda, M.; Long, G.L.; Fan, S.; Nori, F.; Bender, C.M.; Yang, L. Parity-timesymmetric whispering-gallery microcavities. *Nat. Phys.* **2014**, *10*, 394. [CrossRef]
73. Peng, B.; Özdemir, K.; Liertzer, M.; Chen, W.; Kramer, J.; Ylmaz, H.; Wiersig, J.; Rotter, S.; Yang, L. Chiral modes and directional lasing at exceptional points. *Proc. Natl. Acad. Sci. USA* **2016**, *113*, 6845. [CrossRef] [PubMed]
74. Feng, L.; Wong, Z.J.; Ma, R.-M.; Wang, Y.; Zhang, X. Single-mode laser by parity-time symmetry breaking. *Science* **2014**, *346*, 972. [CrossRef] [PubMed]
75. Hodaei, H.; Miri, M.-A.; Heinrich, M.; Christodoulides, D.N.; Khajavikhan, M. Parity-time-symmetric microring lasers. *Science* **2014**, *346*, 975. [CrossRef]
76. Chen, W.; Özdemir, K.; Zhao, G.; Wiersig, J.; Yang, L. Exceptional points enhance sensing in an optical microcavity. *Nature* **2017**, *548*, 192. [CrossRef]
77. Wiersig, J. Enhancing the Sensitivity of Frequency and Energy Splitting Detection by Using Exceptional Points: Application to Microcavity Sensors for Single-Particle Detection. *Phys. Rev. Lett.* **2014**, *112*, 203901. [CrossRef]
78. Hodaei, H.; Hassan, A.U.; Wittek, S.; Garcia-Gracia, H.; El-Ganainy, R.; Christodoulides, D.N.; Khajavikhan, M. Enhanced sensitivity at higher-order exceptional points. *Nature* **2017**, *548*, 187. [CrossRef]
79. Rechtsman, M.C.; Zeuner, J.M.; Plotnik, Y.; Lumer, Y.; Podolsky, D.; Dreisow, F.; Nolte, S.; Segev, M.; Szameit, A. Photonic Floquet topological insulators. *Nature* **2013**, *496*, 196–200. [CrossRef]
80. Noh, J.; Huang, S.; Leykam, D.; Chong, Y.D.; Chen, K.; Rechtsman, M.C. Experimental observation of Weyl points. *Science* **2015**, *349*, 622–625.
81. Noh, J.; Benalcazar, W.A.; Huang, S.; Collins, M.J.; Chen, K.P.; Hughes, T.L.; Rechtsman, M.C. Topological protection of photonic mid-gap defect modes. *Nat. Photonics* **2018**, *12*, 408–415. [CrossRef]
82. El Hassan, A.; Kunst, F.K.; Moritz, A.; Andler, G.; Bergholtz, E.J.; Bourennane, M. Corner states of light in photonic waveguides. *Nat. Photonics* **2019**, *13*, 697–700. [CrossRef]
83. Liu, J.; Li, Z.; Chen, Z.; Tang, W.; Chen, A.; Liang, B.; Ma, G.; Cheng, J. Experimental Realization of Weyl Exceptional Rings in a Synthetic Three-Dimensional Non-Hermitian Phononic Crystal. *Phys. Rev. Lett.* **2019**, *129*, 084301. [CrossRef] [PubMed]
84. Weimann, S.; Kremer, M.; Plotnik, Y.; Lumer, Y.; Nolte, S.; Makris, K.G.; Segev, M.; Rechtsman, M.C.; Szameit, A. Topologically protected bound states in photonic parity-timesymmetric crystals. *Nat. Mater.* **2017**, *16*, 433. [CrossRef] [PubMed]
85. Zeuner, J.M.; Rechtsman, M.C.; Plotnik, Y.; Lumer, Y.; Nolte, S.; Rudner, M.S.; Segev, M.; Szameit, A. Observation of a Topological Transition in the Bulk of a Non-Hermitian System. *Phys. Rev. Lett.* **2015**, *115*, 040402. [CrossRef]
86. Biesenthal, T.; Kremer, M.; Heinrich, M.; Szameit, A. Experimental Realization of PT-Symmetric Flat Bands. *Phys. Rev. Lett.* **2019**, *123*, 183601. [CrossRef]
87. Özdemir, K.; El-Ganainy, R. Topological lattices lit at the corners. *Nat. Photonics* **2019**, *13*, 660–662. [CrossRef]
88. Guo, A.; Salamo, G.J.; Duchesne, D.; Morandotti, R.; Ravat, M.V.; Aimez, V.; Siviloglou, G.A.; Christodoulides, D.N. Observation of PT-Symmetry Breaking in Complex Optical Potentials. *Phys. Rev. Lett.* **2009**, *103*, 093902. [CrossRef]
89. Bai, R.; Zhang, C.; Gu, X.; Jin, X.; Zhang, Y.; Lee, Y. Switching the unidirectional reflectionlessness by polarization in non-ideal PT metamaterial based on the phase coupling. *Sci. Rep.* **2017**, *7*, 10742. [CrossRef]
90. Ornigotti, M.; Szameit, A. Quasi PT-symmetry in passive photonic lattices. *J. Opt.* **2014**, *16*, 065501. [CrossRef]
91. Yuce, C.; Oztas, Z. PT symmetry protected non-Hermitian topological systems. *Sci. Rep.* **2018**, *8*, 17416. [CrossRef]
92. Kremer, M.; Biesenthal, T.; Maczewsky, L.J.; Heinrich, M.; Thomale, R.; Szameit, A. Demonstration of a twodimensional PT -symmetric crystal. *Nat. Commun.* **2019**, *10*, 435. [CrossRef] [PubMed]
93. Regensburger, A.; Bersch, C.; Miri, M.-A.; Onishchukov, G.; Christodoulides, D.N.; Peschel, U. Parity-time synthetic photonic lattices. *Nature* **2012**, *488*, 167. [CrossRef] [PubMed]
94. Li, G.; Zhang, S.; Zentgraf, T. Nonlinear photonic metasurfaces. *Nat. Rev. Phys.* **2017**, *2*, 1. [CrossRef]
95. Smirnova, D.; Leykam, D.; Chong, Y.; Kivshar, Y. Nonlinear topological photonics. *Appl. Phys. Rev.* **2020**, *7*, 021306. [CrossRef]
96. Koshelev, K.; Tonkaev, P.; Kivshar, Y. Nonlinear chiral metaphotonics: A perspective. *Adv. Photons.* **2023**, *6*, 064001. [CrossRef]
97. Timurdogan, E.; Poulton, C.V.; Byrd, M.J.; Watts, M.R. Electric field-induced second-order nonlinear optical effects in silicon waveguides. *Nat. Photonics* **2017**, *11*, 200. [CrossRef]
98. Kirsch, M.S.; Zhang, Y.; Kremer, M.; Maczewsky, L.J.; Ivanov, S.K.; Kartashov, Y.V.; Torner, L.; Bauer, D.; Szameit, A.; Heinrich, M. Nonlinear second-order photonic topological insulators. *Nat. Phys.* **2020**, *17*, 995. [CrossRef]
99. Xia, S.; Kaltsas, D.; Song, D.; Komis, I.; Xu, J.; Szameit, A.; Buljan, H.; Makris, K.G.; Chen, Z. Nonlinear tuning of PT symmetry and non-Hermitian topological states. *Science* **2021**, *372*, 72. [CrossRef]
100. Dai, T.; Ao, Y.; Mao, J.; Yang, Y.; Zheng, Y.; Zhai, C.; Li, Y.; Yuan, J.; Tang, B.; Li, Z.; et al. Non-Hermitian topological phase transitions controlled by nonlinearity. *Nat. Phys.* **2024**, *20*, 101.
101. Ma, W.; Zhuang, Y.; Wang, Z.; Jia, P.; Zhang, P.; Hu, Y.; Chen, Z.; Xu, J. Breaking the action-reaction principle of light interactions under a stroboscopic nonlinearity. *Laser Photonics Rev.* **2023**, *17*, 2200177. [CrossRef]
102. Zhan, J.; Li, D.; Bongiovanni, D.; Xiang, Y.; Chen, S.; Zhang, Y.; Tang, L.; Song, D.; Yang, J.; Morandotti, R.; et al. Nonlinear generation of hollow beams in tunable plasmonic nanosuspensions. *APL Photonics* **2023**, *8*, 076102. [CrossRef]

103. Raymond, A.; Zecchetto, A.; Palomo, J.; Morassi, M.; Lemaître, A.; Raineri, F.; Amanti, M.I.; Ducci, S.; Baboux, F. Tunable Generation of Spatial Entanglement in Nonlinear Waveguide Arrays. *Phys. Rev. Lett.* **2024**, *133*, 233602. [CrossRef]
104. Imhof, S.; Berger, C.; Bayer, F.; Brehm, J.; Molenkamp, L.W.; Kiessling, T.; Schindler, F.; Lee, C.H.; Greiter, M.; Neupert, T.; et al. Topolectrical-circuit realization of topological corner modes. *Nat. Phys.* **2018**, *14*, 925–929. [CrossRef]
105. Helbig, T.; Hofmann, T.; Imhof, S.; Abdelghany, M.; Kiessling, T.; Molenkamp, L.W.; Lee, C.H.; Szameit, A.; Greiter, M.; Thomale, R. Generalized bulk-boundary correspondence in non-Hermitian topolectrical circuits. *Nat. Phys.* **2020**, *16*, 747–750. [CrossRef]
106. Hofmann, T.; Helbig, T.; Schindler, F.; Salgo, N.; Brzezińska, M.; Greiter, M.; Kiessling, T.; Wolf, D.; Vollhardt, A.; Kabaši, A.; et al. Reciprocal skin effect and its realization in a topolectrical circuit. *Phys. Rev. Res.* **2020**, *2*, 023265. [CrossRef]
107. Luo, K.; Feng, J.; Zhao, Y.X.; Yu, R. Nodal manifolds bounded by exceptional points on non-Hermitian honeycomb lattices and electrical-circuit realizations. *arXiv* **2018**, arXiv:1810.09231.
108. Ezawa, M. Electric circuits for non-Hermitian Chern insulators. *Phys. Rev. B* **2019**, *100*, 081401. [CrossRef]
109. Hofmann, T.; Helbig, T.; Lee, C.H.; Greiter, M.; Thomale, R. Chiral Voltage Propagation and Calibration in a Topolectrical Chern Circuit. *Phys. Rev. Lett.* **2019**, *122*, 247702. [CrossRef]
110. Ezawa, M. Non-Hermitian boundary and interface states in nonreciprocal higher-order topological metals and electrical circuits. *Phys. Rev. B* **2019**, *99*, 121411. [CrossRef]
111. Ezawa, M. Non-Hermitian higher-order topological states in nonreciprocal and reciprocal systems with their electric-circuit realization. *Phys. Rev. B* **2019**, *99*, 201411. [CrossRef]
112. Ezawa, M. Electric-circuit simulation of the Schrödinger equation and non-Hermitian quantum walks. *Phys. Rev. B* **2019**, *100*, 165419. [CrossRef]
113. Li, L.; Lee, C.H.; Gong, J. Emergence and full 3Dimaging of nodal boundary Seifert surfaces in 4D topological matter. *Commun. Phys.* **2019**, *2*, 135. [CrossRef]
114. Zhang, X.-X.; Franz, M. Non-Hermitian Exceptional Landau Quantization in Electric Circuits. *Phys. Rev. Lett.* **2020**, *124*, 046401. [CrossRef] [PubMed]
115. Shang, C.; Liu, S.; Shao, R.; Han, P.; Zang, X.; Zhang, X.; Salama, K.N.; Gao, W.; Lee, C.H.; Thomale, R.; et al. Experimental Identification of the Second-Order Non-Hermitian Skin Effect with Physics-Graph-Informed Machine Learning. *Adv. Sci.* **2023**, *9*, 2202922. [CrossRef] [PubMed]
116. Zhang, X.; Zhang, B.; Sahin, H.; Siu, Z.B.; Rafi-Ul-Islam, S.M.; Kong, J.F.; Shen, B.; Jalil, M.B.A.; Thomale, R.; Lee, C.H. Anomalous fractal scaling in two-dimensional electric networks. *Commun. Phys.* **2023**, *6*, 151. [CrossRef]
117. Li, Y.; Sun, Y.; Zhu, W.; Guo, Z.; Jiang, J.; Kariyado, T.; Chen, H.; Hu, X. Topological LC-circuits based on microstrips and observation of electromagnetic modes with orbital angular momentum. *Nat. Commun.* **2018**, *9*, 4598.
118. Long, Y.; Ren, J.; Guo, Z.; Jiang, H.; Wang, Y.; Sun, Y.; Chen, H. Designing All-Electric Subwavelength Metasources for Near-Field Photonic Routings. *Phys. Rev. Lett.* **2020**, *125*, 157401. [CrossRef]
119. Yang, H.; Song, L.; Cao, Y.; Yan, P. Realization of Wilson fermions in topolectrical circuits. *Commun. Phys.* **2023**, *6*, 211.
120. Lee, C.H.; Sutrisno, A.; Hofmann, T.; Helbig, T.; Liu, Y.; Ang, Y.S.; Ang, L.K.; Zhang, X.; Greiter, M.; Thomale, R. Imaging nodal knots in momentum space through topolectrical circuits. *Nat. Commun.* **2020**, *11*, 4385.
121. Bao, J.; Zou, D.; Zhang, W.; He, W.; Sun, H.; Zhang, X. Topoelectrical circuit octupole insulator with topologically protected corner states. *Phys. Rev. B* **2019**, *100*, 201406(R). [CrossRef]
122. Zou, D.; Chen, T.; He, W.; Bao, J.; Lee, C.H.; Sun, H.; Zhang, X. Observation of hybrid higher-order skin-topological effect in non-Hermitian topolectrical circuits. *Nat. Commun.* **2021**, *12*, 7201.
123. Pan, N.; Chen, T.; Ji, T.; Tong, X.; Zhang, X. Three-dimensional non-Abelian Bloch oscillations and higher-order topological states. *Commun. Phys.* **2023**, *6*, 355.
124. Bai, K.; Liu, T.-R.; Fang, L.; Li, J.-Z.; Lin, C.; Wan, D.; Xiao, M. Observation of Nonlinear Exceptional Points with a Complete Basis in Dynamics. *Phys. Rev. Lett.* **2023**, *132*, 073802. [CrossRef] [PubMed]
125. Aharonov, Y.; Davidovich, L.; Zagury, N. Quantum random walks. *Phys. Rev. A* **1993**, *48*, 1687–1690. [CrossRef] [PubMed]
126. Karski, M.; Förster, L.; Choi, J.M.; Steffen, A.; Alt, W.; Meschede, D.; Widera, A. Quantum walk in position space with single optically trapped atoms. *Science* **2009**, *325*, 174–177. [CrossRef]
127. Schmitz, H.; Matjeschk, R.; Schneider, C.; Glueckert, J.; Enderlein, M.; Huber, T.; Schaetz, T. Quantum Walk of a Trapped Ion in Phase Space. *Phys. Rev. Lett.* **2009**, *103*, 090504. [CrossRef]
128. Zähringer, F.; Kirchmair, G.; Gerritsma, R.; Solano, E.; Blatt, R.; Roos, C.F. Realization of a Quantum Walk with One and Two Trapped Ions. *Phys. Rev. Lett.* **2010**, *104*, 100503. [CrossRef]
129. Broome, M.A.; Fedrizzi, A.; Lanyon, B.P.; Kassal, I.; Guzik, A.A.; White, A.G. Discrete Single-Photon Quantum Walks with Tunable Decoherence. *Phys. Rev. Lett.* **2010**, *104*, 153602. [CrossRef]
130. Schreiber, A.; Cassemiro, K.N.; Potoček, V.; Gábris, A.; Mosley, P.J.; Andersson, E.; Jex, I.; Silberhorn, C. Photons Walking the Line: A Quantum Walk with Adjustable Coin Operations. *Phys. Rev. Lett.* **2010**, *104*, 050502. [CrossRef]
131. Ryan, C.A.; Laforest, M.; Boileau, J.C.; Laflamme, R. Experimental implementation of a discrete-time quantum random walk on an NMR quantum-information processor. *Phys. Rev. A* **2005**, *72*, 062317. [CrossRef]
132. Kitagawa, T.; Rudner, M.S.; Berg, E.; Demler, E. Exploring topological phases with quantum walks. *Phys. Rev. A* **2010**, *82*, 033429. [CrossRef]

133. Asbóth, J.K. Symmetries, topological phases, and bound states in the one-dimensional quantum walk. *Phys. Rev. B* **2012**, *86*, 195414. [CrossRef]
134. Kitagawa, T.; Broome, M.A.; Fedrizzi, A.; Rudner, M.S.; Berg, E.; Kassal, I.; Aspuru-Guzik, A.; Demler, E.; White, A.G. Observation of topologically protected bound states in photonic quantum walks. *Nat. Commun.* **2012**, *3*, 882. [CrossRef] [PubMed]
135. Cardano, F.; Maffei, M.; Massa, F.; Piccirillo, B.; De Lisio, C.; De Filippis, G.; Cataudella, V.; Santamato, E.; Marrucci, L. Statistical moments of quantum-walk dynamics reveal topological quantum transitions. *Nat. Commun.* **2016**, *7*, 11439. [CrossRef]
136. Barkhofen, S.; Nitsche, T.; Elster, F.; Lorz, L.; Gábris, A.; Jex, I.; Silberhorn, C. Measuring topological invariants in disordered discrete-time quantum walks. *Phys. Rev. A* **2017**, *96*, 033846. [CrossRef]
137. Flurin, E.; Ramasesh, V.V.; Hacohen-Gourgy, S.; Martin, L.S.; Yao, N.Y.; Siddiqi, I. Observing Topological Invariants Using Quantum Walks in Superconducting Circuits. *Phys. Rev. X* **2017**, *7*, 031023. [CrossRef]
138. Ramasesh, V.V.; Flurin, E.; Rudner, M.; Siddiqi, I.; Yao, N.Y. Direct Probe of Topological Invariants Using Bloch Oscillating Quantum Walks. *Phys. Rev. Lett.* **2017**, *118*, 130501. [CrossRef]
139. Chen, T.; Zhang, X. The defect-induced localization in many positions of the quantum random walk. *Sci. Rep.* **2016**, *6*, 25767. [CrossRef]
140. Chen, T.; Wang, B.; Zhang, X. Characterization of topological phases and selection of topological interface modes in the parity-time-symmetric quantum walk. *Phys. Rev. A* **2018**, *97*, 052117. [CrossRef]
141. Chen, T.; Zhang, X.; Zhang, X. Quantum sensing of noises in one and two dimensional quantum walks. *Sci. Rep.* **2017**, *7*, 4962. [CrossRef]
142. Chen, T.; Wang, B.; Zhang, X. Controlling probability transfer in the discrete-time quantum walk by modulating the symmetries. *New J. Phys.* **2017**, *19*, 113049. [CrossRef]
143. Rudner, M.S.; Levitov, L.S. Topological Transition in a Non-Hermitian Quantum Walk. *Phys. Rev. Lett.* **2009**, *102*, 065703. [CrossRef] [PubMed]
144. Xiao, L.; Bian, Z.H.; Wang, K.K.; Zhang, X.; Wang, X.P.; Li, J.; Mochizuki, K.; Kim, D.; Kawakami, N.; Yi, W.; et al. Observation of topological edge states in parity-time-symmetric quantum walks. *Nat. Phys.* **2017**, *13*, 1117–1123. [CrossRef]
145. Mochizuki, K.; Kim, D.; Obuse, H. Explicit definition of PT symmetry for nonunitary quantum walks with gain and loss. *Phys. Rev. A* **2016**, *93*, 062116. [CrossRef]
146. Wang, K.; Qiu, X.; Xiao, L.; Zhan, X.; Bian, Z.; Sanders, B.C.; Yi, W.; Xue, P. Observation of emergent momentum-time skyrmions in parity-time-symmetric non-unitary quench dynamics. *Nat. Commun.* **2019**, *10*, 2293. [CrossRef]
147. Longhi, S. Non-Bloch PT symmetry breaking in non-Hermitian photonic quantum walks. *Opt. Lett.* **2019**, *44*, 5804. [CrossRef]
148. Wang, B.; Chen, T.; Zhang, X. Observation of Novel Robust Edge States in Dissipative Non-Hermitian Quantum Walks. *Laser Photonics Rev.* **2020**, *14*, 2000092. [CrossRef]
149. Zhang, R.; Liu, Y.; Chen, T. Non-Hermiticity-induced quantum control of localization in quantum walks. *Phys. Rev. A* **2020**, *102*, 022218. [CrossRef]
150. Chen, T.; Zhang, S.; Zhang, Y.; Liu, Y.; Kou, S.; Sun, H.; Zhang, X. Experimental observation of classical analogy of topological entanglement entropy. *Nat. Commun.* **2019**, *10*, 1557. [CrossRef]
151. Zhang, R.; Chen, T. Fast quantum search driven by environmental engineering. *Commun. Theor. Phys.* **2022**, *74*, 045101. [CrossRef]
152. Zhang, R.; Chen, T. True exponentially enhanced sensing in the non-Hermitian topological phase. *Appl. Phys. Lett.* **2024**, *124*, 174002. [CrossRef]
153. Weidemann, S.; Kremer, M.; Helbig, T.; Hofmann, T.; Stegmaier, A.; Greiter, M.; Thomale, R.; Szameit, A. Topological funneling of light. *Science* **2020**, *368*, 311–314. [CrossRef]
154. Xiao, L.; Deng, T.; Wang, K.; Zhu, G.; Wang, Z.; Yi, W.; Xue, P. Non-Hermitian bulk-boundary correspondence in quantum dynamics. *Nat. Phys.* **2020**, *16*, 761–766. [CrossRef]
155. Xu, X.; Wang, Q.; Heyl, M.; Budich, J.C.; Pan, W.; Chen, Z.; Jan, M.; Sun, K.; Xu, J.; Han, Y.; et al. Measuring a dynamical topological order parameter in quantum walks. *Light Sci. Appl.* **2020**, *9*, 7. [CrossRef]
156. Bagrets, D.; Kim, K.W.; Barkhofen, S.; De, S.; Sperling, J.; Silberhorn, C.; Altland, A.; Micklitz, T. Probing the topological Anderson transition with quantum walks. *Phys. Rev. Res.* **2021**, *3*, 023183. [CrossRef]
157. Lin, Q.; Li, T.; Xiao, L.; Wang, K.; Yi, W.; Xue, P. Observation of non-Hermitian topological Anderson insulator in quantum dynamics. *Nat. Commun.* **2022**, *13*, 3229. [CrossRef]
158. Chen, C.; Ding, X.; Qin, J.; Wu, J.; He, Y.; Lu, C.-Y.; Li, L.; Liu, X.-J.; Sanders, B.C.; Pan, J.-W. Topological Spin Texture of Chiral Edge States in Photonic Two-Dimensional Quantum Walks. *Phys. Rev. Lett.* **2022**, *129*, 046401. [CrossRef]
159. Klauck, F.; Heinrich, M.; Szameit, A. Photonic two-particle quantum walks in Su–Schrieffer–Heeger lattices. *Photonics Res.* **2021**, *9*, A1. [CrossRef]
160. Süsstrunk, R.; Huber, S.D. Classification of topological phonons in linear mechanical metamaterials. *Proc. Natl. Acad. Sci. USA* **2016**, *113*, E4767–E4775. [CrossRef]
161. Kane, C.L.; Lubensky, T.C. Topological boundary modes in isostatic lattices. *Nat. Phys.* **2014**, *10*, 39–45. [CrossRef]
162. Chen, B.G.G.; Upadhyaya, N.; Vitelli, V. Nonlinear conduction via solitons in a topological mechanical insulator. *Proc. Natl. Acad. Sci. USA* **2014**, *111*, 13004–13009. [CrossRef] [PubMed]
163. Paulose, J.; Chen, B.G.G.; Vitelli, V. Topological modes bound to dislocations in mechanical metamaterials. *Nat. Phys.* **2015**, *11*, 153–156. [CrossRef]

164. Nash, L.M.; Kleckner, D.; Read, A.; Vitelli, V.; Turner, A.M.; Irvine, W.T.M. Topological mechanics of gyroscopic metamaterials. *Proc. Natl. Acad. Sci. USA* **2015**, *112*, 14495–14500. [CrossRef] [PubMed]
165. Wang, P.; Lu, L.; Bertoldi, K. Topological Phononic Crystals with One-Way Elastic Edge Waves. *Phys. Rev. Lett.* **2015**, *115*, 104302. [CrossRef]
166. Brandenbourger, M.; Locsin, X.; Lerner, E.; Coulais, C. Non-reciprocal robotic metamaterials. *Nat. Commun.* **2019**, *10*, 4608. [CrossRef]
167. Ghatak, A.; Brandenbourger, M.; van Wezel, J.; Coulais, C. Observation of non-Hermitian topology and its bulk-edge correspondence in an active mechanical metamaterial. *Proc. Natl. Acad. Sci. USA* **2020**, *117*, 29561–29568. [CrossRef]
168. Schomerus, H. Nonreciprocal response theory of non-Hermitian mechanical metamaterials: Response phase transition from the skin effect of zero modes. *Phys. Rev. Res.* **2020**, *2*, 013058. [CrossRef]
169. Rosa, M.I.N.; Ruzzene, M. Dynamics and topology of non-Hermitian elastic lattices with non-local feedback control interactions. *New J. Phys.* **2020**, *22*, 053004. [CrossRef]
170. Scheibner, C.; Souslov, A.; Banerjee, D.; Surowka, P.; Irvine, W.T.M.; Vitelli, V. Odd elasticity. *Nat. Phys.* **2020**, *16*, 475. [CrossRef]
171. Zhou, D.; Zhang, J. Non-Hermitian topological metamaterials with odd elasticity. *Phys. Rev. Res.* **2020**, *2*, 023173. [CrossRef]
172. Scheibner, C.; Irvine, W.T.M.; Vitelli, V. Non-Hermitian Band Topology and Skin Modes in Active Elastic Media. *Phys. Rev. Lett.* **2020**, *125*, 118001. [CrossRef] [PubMed]
173. Yoshida, T.; Hatsugai, Y. Exceptional rings protected by emergent symmetry for mechanical systems. *Phys. Rev. B* **2019**, *100*, 054109. [CrossRef]
174. Kushwaha, M.S.; Halevi, P.; Dobrzynski, L.; Djafari-Rouhani, B. Acoustic Band Structure of Periodic Elastic Composites. *Phys. Rev. Lett.* **1993**, *71*, 2022–2025. [CrossRef] [PubMed]
175. Prodan, E.; Prodan, C. Topological Phonon Modes and Their Role in Dynamic Instability of Microtubules. *Phys. Rev. Lett.* **2009**, *103*, 248101. [CrossRef]
176. Mousavi, S.H.; Khanikaev, A.B.; Wang, Z. Topologically protected elastic waves in phononic metamaterials. *Nat. Commun.* **2015**, *6*, 8682. [CrossRef]
177. He, H.; Qiu, C.; Ye, L.; Cai, X.; Fan, X.; Ke, M.; Zhang, F.; Liu, Z. Topological negative refraction of surface acoustic waves in a Weyl phononic crystal. *Nature* **2018**, *560*, 61–64. [CrossRef]
178. Yang, Z.; Gao, F.; Shi, X.; Lin, X.; Gao, Z.; Chong, Y.; Zhang, B. Topological Acoustics. *Phys. Rev. Lett.* **2015**, *114*, 114301. [CrossRef]
179. Shi, C.; Dubois, M.; Chen, Y.; Cheng, L.; Ramezani, H.; Wang, Y.; Zhang, X. Accessing the exceptional points of parity-time symmetric acoustics. *Nat. Commun.* **2016**, *7*, 11110. [CrossRef]
180. Aur, Y.; Pagneux, V. PT-Symmetric Scattering in Flow Duct Acoustics. *Phys. Rev. Lett.* **2017**, *118*, 174301.
181. Rivet, E.; Brandstötter, A.; Makris, K.G.; Lissek, H.; Rotter, S.; Fleury, R. Constant-pressure sound waves in non-Hermitian disordered media. *Nat. Phys.* **2018**, *14*, 942–947. [CrossRef]
182. Zhu, W.; Fang, X.; Li, D.; Sun, Y.; Li, Y.; Jing, Y.; Chen, H. Simultaneous Observation of a Topological Edge State and Exceptional Point in an Open and Non-Hermitian Acoustic System. *Phys. Rev. Lett.* **2018**, *121*, 124501. [CrossRef] [PubMed]
183. López, M.R.; Zhang, Z.; Torrent, D.; Christensen, J. Multiple scattering theory of non-Hermitian sonic second-order topological insulators. *Commun. Phys.* **2019**, *2*, 132. [CrossRef]
184. Zhang, Z.; López, M.R.; Cheng, Y.; Liu, X.; Christensen, J. Non-Hermitian Sonic Second-Order Topological Insulator. *Phys. Rev. Lett.* **2019**, *122*, 195501. [CrossRef]
185. Fleury, R.; Sounas, D.; Alù, A. An invisible acoustic sensor based on parity-time symmetry. *Nat. Commun.* **2015**, *6*, 5905. [CrossRef]
186. Chen, Z.G.; Zhang, R.Y.; Chan, C.T.; Ma, G. Classical non-Abelian braiding of acoustic modes. *Nat. Phys.* **2022**, *18*, 179.
187. Zhang, X.L.; Yu, F.; Chen, Z.G.; Tian, Z.N.; Chen, Q.D.; Sun, H.B.; Ma, G. Non-Abelian braiding on photonic chips. *Nat. Photonics* **2022**, *16*, 390. [CrossRef]
188. Xue, H.; Yang, Y.; Zhang, B. Topological acoustics. *Nat. Rev. Mater.* **2022**, *7*, 974. [CrossRef]
189. Zhang, X.; Zangeneh-Nejad, F.; Chen, Z.-G.; Lu, M.-H.; Christensen, J. A second wave of topological phenomena in photonics and acoustics. *Nature* **2023**, *618*, 687. [CrossRef]
190. Lin, Z.-K.; Wang, Q.; Liu, Y.; Xue, H.; Zhang, B.; Chong, Y.; Jiang, J.-H. Topological phenomena at defects in acoustic, photonic and solid-state lattices. *Nat. Rev. Phys.* **2023**, *5*, 483. [CrossRef]
191. Majorana, E. Sulla formazione dello ione molecolare dielio. *Nuovo Cimento* **1931**, *8*, 22–28. [CrossRef]
192. Feshbach, H.; Porter, C.E.; Weisskopf, V.F. Model for nuclear reactions with neutrons. *Phys. Rev.* **1954**, *96*, 448–464. [CrossRef]
193. Feshbach, H. Unified theory of nuclear reactions. *Ann. Phys* **1958**, *5*, 357–390. [CrossRef]
194. Fano, U. Effects of configuration interaction on intensities and phase shifts. *Phys. Rev.* **1961**, *124*, 1866–1878. [CrossRef]
195. Rotter, I. A non-Hermitian Hamilton operator and the physics of open quantum systems. *J. Phys. A* **2009**, *42*, 153001. [CrossRef]
196. Carmichael, H. *An Open Systems Approach to Quantum Optics Lectures Presented at the Université Libre de Bruxelles, October 28 to November 4, 1991*; Springer: Berlin, Germany, 2014.
197. Chen, T.; Wang, X. Fast cooling in dispersively and dissipatively coupled optomechanics. *Sci. Rep.* **2015**, *5*, 7745. [CrossRef]
198. Zhang, R.; Chen, T.; Wang, X. Deterministic quantum controlled-PHASE gates based on non-Markovian environments. *New J. Phys.* **2017**, *19*, 123001. [CrossRef]
199. Diehl, S.; Rico, E.; Baranov, M.A.; Zoller, P. Topology by dissipation in atomic quantum wires. *Nat. Phys.* **2011**, *7*, 971–977. [CrossRef]

200. Eisert, J.; Prosen, T. Noise-driven quantum criticality. *arXiv* **2010**, arXiv:1012.5013.
201. Prosen, T. Spectral theorem for the Lindblad equation for quadratic open fermionic systems. *J. Stat. Mech.* **2010**, *2010*, P07020. [CrossRef]
202. Song, F.; Yao, S.; Wang, Z. Non-Hermitian Skin Effect and Chiral Damping in Open Quantum Systems. *Phys. Rev. Lett.* **2019**, *123*, 170401. [CrossRef]
203. Watatsuki, R.; Ezawa, M.; Nagaosa, N. Domain wall of a ferromagnet on a three-dimensional topological insulator. *Sci. Rep.* **2015**, *5*, 13638.
204. Datta, S. *Quantum Transport: Atom to Transistor*; Cambridge University Press: Cambridge, UK, 2005; Volume 9780521631.
205. Pikulin, D.I.; Nazarov, Y.V. Topological properties of superconducting junctions. *JETP Lett.* **2012**, *94*, 693–697. [CrossRef]
206. Pikulin, D.I.; Nazarov, Y.V. Two types of topological transitions in finite Majorana wires. *Phys. Rev. B* **2013**, *87*, 235421. [CrossRef]
207. San-Jose, P.; Cayao, J.; Prada, E.; Aguado, R. Majorana bound states from exceptional points in non-topological superconductors. *Sci. Rep.* **2016**, *6*, 21427. [CrossRef] [PubMed]
208. Avila, J.; Peñaranda, F.; Prada, E.; San-Jose, P.; Aguado, R. Non-Hermitian topology as a unifying framework for the Andreev versus Majorana states controversy. *Commun. Phys.* **2019**, *2*, 133. [CrossRef]
209. Chen, Y.; Zhai, H. Hall conductance of a non-Hermitian Chern insulator. *Phys. Rev. B* **2018**, *98*, 245130. [CrossRef]
210. Philip, T.M.; Hirsbrunner, M.R.; Gilbert, M.J. Loss of Hall conductivity quantization in a non-Hermitian quantum anomalous Hall insulator. *Phys. Rev. B* **2018**, *98*, 155430. [CrossRef]
211. McDonald, A.; Pereg-Barnea, T.; Clerk, A.A. Phase-Dependent Chiral Transport and Effective Non-Hermitian Dynamics in a Bosonic Kitaev-Majorana Chain. *Phys. Rev. X* **2018**, *8*, 041031. [CrossRef]
212. Wang, Y.X.; Clerk, A.A. Non-Hermitian dynamics without dissipation in quantum systems. *Phys. Rev. A* **2019**, *99*, 063834. [CrossRef]
213. Eckardt, A. Colloquium: Atomic quantum gases in periodically driven optical lattices. *Rev. Mod. Phys.* **2017**, *89*, 011004. [CrossRef]
214. Li, L.; Lee, C.H.; Gong, J. Topological Switch for Non-Hermitian Skin Effect in Cold-Atom Systems with Loss. *Phys. Rev. Lett.* **2020**, *124*, 250402. [CrossRef] [PubMed]
215. Haga, T.; Nakagawa, M.; Hamazaki, R.; Ueda, M. Liouvillian Skin Effect: Slowing Down of Relaxation Processes without Gap Closing. *Phys. Rev. Lett.* **2021**, *127*, 070402. [CrossRef]
216. Yang, F.; Jiang, Q.-D.; Bergholtz, E.J. Liouvillian skin effect in an exactly solvable model. *Phys. Rev. Res.* **2022**, *4*, 023160. [CrossRef]
217. Chen, W.; Abbasi, M.; Ha, B.; Erdamar, S.; Joglekar, Y.N.; Murch, K.W. Decoherence-Induced Exceptional Points in a Dissipative Superconducting Qubit. *Phys. Rev. Lett.* **2022**, *128*, 110402. [CrossRef]
218. Abbasi, M.; Chen, W.; Naghiloo, M.; Joglekar, Y.N.; Murch, K.W. Topological Quantum State Control through Exceptional-Point Proximity. *Phys. Rev. Lett.* **2022**, *128*, 160401. [CrossRef]
219. Gliozzi, J.; De Tomasi, G.; Hughes, T.L. Many-Body Non-Hermitian Skin Effect for Multipoles. *Phys. Rev. Lett.* **2024**, *133*, 136503. [CrossRef]
220. Leykam, D.; Bliokh, K.; Huang, C.; Chong, Y.; Nori, F. Edge Modes, Degeneracies, and Topological Numbers in Non-Hermitian Systems. *Phys. Rev. Lett.* **2017**, *118*, 040401. [CrossRef]
221. Gong, J.; Wang, Q. Stabilizing Non-Hermitian Systems by Periodic Driving. *Phys. Rev. A* **2015**, *91*, 042135. [CrossRef]
222. Zyuzin, A.A.; Simon, P. Disorder-induced exceptional points and nodal lines in Dirac superconductors. *Phys. Rev. B* **2019**, *99*, 165145. [CrossRef]
223. Michishita, Y.; Peters, R. Equivalence of Effective Non-Hermitian Hamiltonians in the Context of Open Quantum Systems and Strongly Correlated Electron Systems. *Phys. Rev. Lett.* **2020**, *124*, 196401. [CrossRef]
224. Deutsch, J.M. Quantum statistical mechanics in a closed system. *Phys. Rev. A* **1991**, *43*, 2046–2049. [CrossRef] [PubMed]
225. Srednicki, M. Chaos and quantum thermalization. *Phys. Rev. E* **1994**, *50*, 888–901. [CrossRef] [PubMed]
226. Chen, C.; Song, J.; Jiang, H.; Sun, Q.; Wang, Z.; Xie, X. Disorder and metal-insulator transitions in Weyl semimetals. *Phys. Rev. Lett.* **2015**, *115*, 246603. [CrossRef] [PubMed]
227. Xu, Q.; Yu, R.; Fang, Z.; Dai, X.; Weng, H. Topological nodal line semimetals in the CaP3 family of materials. *Phys. Rev. B* **2017**, *95*, 045136. [CrossRef]
228. Moors, K.; Zyuzin, A.A.; Zyuzin, A.Y.; Tiwari, R.P.; Schmidt, T.L. Disorder-driven exceptional lines and Fermi ribbons in tilted nodal-line semimetals. *Phys. Rev. B* **2019**, *99*, 041116. [CrossRef]
229. Wang, C.; Lin, C.; Gu, Z. Interacting fermionic symmetry-protected topological phases in two dimensions. *Phys. Rev. B* **2017**, *95*, 195147. [CrossRef]
230. Michishita, Y.; Yoshida, T.; Peters, R. Relationship between exceptional points and the Kondo effect in f-electron materials. *Phys. Rev. B* **2020**, *101*, 085122. [CrossRef]
231. Molina, R.A.; González, J. Surface and 3D Quantum Hall Effects from Engineering of Exceptional Points in Nodal-Line Semimetals. *Phys. Rev. Lett.* **2018**, *120*, 146601. [CrossRef]
232. González, J.; Molina, R.A. Topological protection from exceptional points in Weyl and nodal-line semimetals. *Phys. Rev. B* **2017**, *96*, 045437. [CrossRef]
233. Ghatak, A.; Das, T. Theory of superconductivity with non-Hermitian and parity-time reversal symmetric Cooper pairing symmetry. *Phys. Rev. B* **2018**, *97*, 014512. [CrossRef]
234. Heiss, W.D. Phases of wave functions and level repulsion. *Eur. Phys. J. D-At. Mol. Opt. Plasma Phys.* **1999**, *7*, 1–4. [CrossRef]

235. Uzdin, R.; Mailybaev, A.; Moiseyev, N. On the observability and asymmetry of adiabatic state flips generated by exceptional points. *J. Phys. A Math. Theor.* **2011**, *44*, 435302. [CrossRef]
236. Milburn, T.J.; Doppler, J.; Holmes, C.A.; Portolan, S.; Rotter, S.; Rabl, P. General description of quasiadiabatic dynamical phenomena near exceptional points. *Phys. Rev. A* **2015**, *92*, 052124. [CrossRef]
237. Xu, H.; Mason, D.; Jiang, L.; Harris, J.G.E. Topological energy transfer in an optomechanical system with exceptional points. *Nature* **2016**, *537*, 80–83. [CrossRef]
238. Doppler, J.; Mailybaev, A.A.; Böhm, J.; Kuhl, U.; Girschik, A.; Libisch, F.; Milburn, T.J.; Rabl, P.; Moiseyev, N.; Rotter, S. Dynamically encircling an exceptional point for asymmetric mode switching. *Nature* **2016**, *537*, 76–79. [CrossRef]
239. Schumer, A.; Liu, Y.G.N.; Leshin, J.; Ding, L.; Alahmadi, Y.; Hassan, A.U.; Nasari, H.; Rotter, S.; Christodoulides, D.N.; LiKamWa, P.; et al. Topological modes in a laser cavity through exceptional state transfer. *Science* **2022**, *375*, 884–888. [CrossRef]
240. Persson, E.; Rotter, I.; Stöckmann, H.-J.; Barth, M. Observation of resonance trapping in an open microwave cavity. *Phys. Rev. Lett.* **2000**, *85*, 2478. [CrossRef]
241. Dembowski, C.; Gräf, H.-D.; Harney, H.L.; Heine, A.; Heiss, W.D.; Rehfeld, H.; Richter, A. Experimental observation of the topological structure of exceptional points. *Phys. Rev. Lett.* **2001**, *86*, 787. [CrossRef]
242. Zhang, X.-L.; Wang, S.; Hou, B.; Chan, C.T. Dynamically encircling exceptional points: In situ control of encircling loops and the role of the starting point. *Phys. Rev. X* **2018**, *8*, 021066. [CrossRef]
243. Liu, W.; Wu, Y.; Duan, C.-K.; Rong, X.; Du, J. Dynamically encircling an exceptional point in a real quantum system. *Phys. Rev. Lett.* **2021**, *126*, 170506. [CrossRef]
244. Li, Y.; Peng, Y.-G.; Han, L.; Miri, M.-A.; Li, W.; Xiao, M.; Zhu, X.-F.; Zhao, J.; Alù, A.; Fan, S.; et al. Anti–parity-time symmetry in diffusive systems. *Science* **2019**, *364*, 170–173. [CrossRef] [PubMed]
245. Peng, P.; Cao, W.; Shen, C.; Qu, W.; Wen, J.; Jiang, L.; Xiao, Y. Anti-parity–time symmetry with flying atoms. *Nat. Phys.* **2016**, *12*, 1139–1145. [CrossRef]
246. Yang, Y.; Wang, Y.-P.; Rao, J.W.; Gui, Y.S.; Yao, B.M.; Lu, W.; Hu, C.-M. Unconventional singularity in anti-parity-time symmetric cavity magnonics. *Phys. Rev. Lett.* **2020**, *125*, 147202. [CrossRef]
247. Wu, H.C.; Jin, L.; Song, Z. Topology of an anti-parity-time symmetric non-Hermitian Su-Schrieffer-Heeger model. *Phys. Rev. B* **2021**, *103*, 235110. [CrossRef]
248. Zhang, X.L.; Jiang, T.; Chan, C.T. Dynamically encircling an exceptional point in anti-parity-time symmetric systems: Asymmetric mode switching for symmetry-broken modes. *Light. Sci. Appl.* **2019**, *8*, 88. [CrossRef]
249. Liu, Q.; Li, S.; Wang, B.; Ke, S.; Qin, C.; Wang, K.; Liu, W.; Gao, D.; Berini, P.; Lu, P. Efficient mode transfer on a compact silicon chip by encircling moving exceptional points. *Phys. Rev. Lett.* **2020**, *124*, 153903. [CrossRef]
250. Li, A.; Dong, J.; Wang, J.; Cheng, Z.; Ho, J.S.; Zhang, D.; Wen, J.; Zhang, X.-L.; Chan, C.T.; Alù, A.; et al. Hamiltonian hopping for efficient chiral mode switching in encircling exceptional points. *Phys. Rev. Lett.* **2020**, *125*, 187403. [CrossRef]
251. Blanco-Redondo, A.; Bell, B.; Oren, D.; Eggleton, B.J.; Segev, M. Topological protection of biphoton states. *Science* **2018**, *362*, 568–571. [CrossRef]
252. Wang, M.; Doyle, C.; Bell, B.; Collins, M.J.; Magi, E.; Eggleton, B.J.; Segev, M.; Blanco-Redondo, A. Topologically protected entangled photonic states. *Nanophotonics* **2019**, *8*, 1327–1335. [CrossRef]
253. Wang, Y.; Pang, X.-L.; Lu, Y.-H.; Gao, J.; Chang, Y.-J.; Qiao, L.-F.; Jiao, Z.-Q.; Tang, H.; Jin, X.-M. Topological protection of two-photon quantum correlation on a photonic chip. *Optica* **2019**, *6*, 955–960. [CrossRef]
254. Wang, Y.; Lu, Y.-H.; Gao, J.; Chang, Y.-J.; Ren, R.-J.; Jiao, Z.-Q.; Zhang, Z.-Y.; Jin, X.-M. Topologically protected polarization quantum entanglement on a photonic chip. *Chip* **2022**, *1*, 100003. [CrossRef]
255. Wang, B.; Tang, Z.; Chen, T.; Zhang, X. Nearly Perfect Transmission and Transformation of Entangled States in Topologically Protected Channels. *Laser Photonics Rev.* **2022**, *16*, 2100519. [CrossRef]
256. Tang, Z.; Wang, B.; Chen, T.; Zhang, X. Transmission and transformation of entangled states with high fidelity in a non-Hermitian system. *Phys. Rev. Res.* **2022**, *4*, 043144. [CrossRef]
257. Tang, Z.; Chen, T.; Zhang, X. Highly efficient transfer of quantum state and robust generation of entanglement state around exceptional lines. *Laser Photonics Rev.* **2023**, *18*, 2300794. [CrossRef]
258. Tang, Z.; Chen, T.; Tang, X.; Zhang, X. Topologically protected entanglement switching around exceptional points. *Light. Sci. Appl.* **2024**, *13*, 167. [CrossRef]
259. Wang, Z.; Wang, X.; Hu, Z.; Bongiovanni, D.; Jukić, D.; Tang, L.; Song, D.; Morandotti, R.; Chen, Z.; Buljan, H. Sub-symmetry protected topological states. *Nat. Phys.* **2023**, *19*, 992. [CrossRef]
260. Hu, Z.; Bongiovanni, D.; Wang, Z.; Wang, X.; Song, D.; Xu, J.; Morandotti, R.; Buljan, H.; Chen, Z. Topologically protected vortex transport via chiral-symmetric disclination. *Nat. Photonics* **2024**. [CrossRef]
261. Xie, Y.; Yan, W.; Xia, S.; Liang, Y.; Tang, L.; Song, D.; Xu, J.; Chen, Z. Realization of Topological Corner States in Tailored Photonic Graphene. *ACS Photonics* **2024**, *11*, 772. [CrossRef]
262. Koh, J.M.; Tai, T.; Lee, C.H. Realization of higher-order topological lattices on a quantum computer. *Nat. Commun.* **2024**, *15*, 5807. [CrossRef]
263. Koh, J.M.; Tai, T.; Lee, C.H. Simulation of Interaction-Induced Chiral Topological Dynamics on a Digital Quantum Computer. *Phys. Rev. Lett.* **2022**, *129*, 140502. [CrossRef]

264. Chen, T.; Zou, D.; Zhou, Z.; Wang, R.; Feng, Y.; Sun, H.; Zhang, X. Ultra-sensitivity in reconstructed exceptional systems. *Natl. Sci. Rev.* **2024**, *11*, nwae278. [CrossRef] [PubMed]
265. Zou, D.; Chen, T.; Meng, H.; Ang, Y.S.; Zhang, X.; Lee, C.H. Experimental observation of exceptional bound states in a classical circuit network. *Sci. Bull.* **2024**, *69*, 2194. [CrossRef] [PubMed]
266. Poboiko, I.; Gornyi, I.V.; Mirlin, A.D. Measurement-Induced Phase Transition for Free Fermions above One Dimension. *Phys. Rev. Lett.* **2024**, *132*, 110403. [CrossRef]
267. Cao, W.; Wang, C.; Chen, W.; Hu, S.; Wang, H.; Yang, L.; Zhang, X. Fully integrated parity-timesymmetric electronics. *Nat. Nanotechnol.* **2022**, *17*, 262–268. [CrossRef]
268. Zhu, H.; Chen, H.; Li, S.; Chen, T.; Li, Y.; Luo, X.; Gao, F.; Li, Q.; Zhou, L.; Karim, M.F.; et al. A Dynamically Programmable Quantum Photonic Microprocessor for Graph Computation. *Laser Photonics Rev.* **2023**, *18*, 2300304. [CrossRef]
269. Zhu, H.H.; Chen, H.S.; Chen, T.; Li, Y.; Luo, S.B.; Luo, X.S.; Gao, F.; Li, Q.; Cai, H.; Chin, L.K.; et al. Quantum photonic solver for complicated vibronic spectra of large molecules. *Nat. Commun.* **2024**, *15*, 6057. [CrossRef]